

rijkswaterstaat

# communications

sutrench-model

two-dimensional vertical mathematical  
model for sedimentation in dredged  
channels and trenches by currents  
and waves

by

I. C. van Rijn and G. I. Tan

no. 41/1985

B 3297  
1e ex.

## sutrench-model

two-dimensional vertical mathematical  
model for sedimentation in dredged  
channels and trenches by currents  
and waves

by  
I. c. van rijn of delft hydraulics laboratory  
and  
g. I. tan of locks and weirs department, rijkswaterstaat

the hague, 1985

REF. NR. 4000	DATUM 15-1986
SIGN. B3297e ex	5203 17.0.00
Bibliotiek Rijkswaterstaat v. d. Waterstaat Koningsskade 4 2506 AA 's-Gravenhage	

*all correspondence and applications should be adressed to:*

rijkswaterstaat

dienst getijdewateren

hooftskade 1

postbus 20907

2500 EX the hague – the netherlands

*the views in this article are the author's own.*

recommended catalogue entry:

recommended catalogue entry:

**rijn, i. c. van**

sutrench model : two-dimensional vertical mathematical model for sedimentation in dredged channels and trenches by currents and waves / i. c. van rijn and g. i. tan ; rijkswaterstaat. – the hague : rijkswaterstaat, 1985. – 63 p. : ill. ; 24 cm. – (rijkswaterstaat communications ; no. 41)  
bibliogr.: p. 59–60.

# Contents

	page
Symbols . . . . .	6
Subscripts . . . . .	8
<b>1 Introduction . . . . .</b>	<b>9</b>
<b>2 Basic equations and simplifications for local suspended sediment . . . . .</b>	<b>10</b>
2.1 Continuity equation for constant width . . . . .	10
2.2 Continuity equation for varying width . . . . .	11
<b>3 Flow velocity profiles . . . . .</b>	<b>12</b>
3.1 Introduction . . . . .	12
3.2 Velocity profiles for complicated flows (PROFILE model) . . . . .	12
3.2.1 Longitudinal flow velocity . . . . .	13
3.2.2 Computation procedure . . . . .	16
3.2.3 Calibration . . . . .	16
3.2.4 Vertical flow velocity . . . . .	18
3.2.5 Bed-shear velocity . . . . .	18
3.3 Velocity profiles for gradually varying flows with waves . . . . .	19
3.3.1 Longitudinal flow velocity . . . . .	19
3.3.2 Vertical flow velocity . . . . .	20
<b>4 Fluid and sediment mixing coefficient . . . . .</b>	<b>22</b>
4.1 Introduction . . . . .	22
4.2 Mixing coefficients for complicated flows (PROFILE model) . . . . .	22
4.2.1 Vertical distribution of fluid mixing coefficient . . . . .	22
4.2.2 Longitudinal distribution of fluid mixing coefficient . . . . .	22
4.2.3 Calibration . . . . .	24
4.3 Mixing coefficients for gradually varying flows with waves . . . . .	25
4.3.1 Current alone . . . . .	25
4.3.2 Waves alone . . . . .	26

4.3.3	Current and waves . . . . .	27
4.4	Equilibrium concentration profiles . . . . .	28
<b>5</b>	<b>Boundary conditions . . . . .</b>	<b>29</b>
5.1	Flow domain . . . . .	29
5.2	Inlet boundary . . . . .	29
5.3	Outlet boundary . . . . .	29
5.4	Water surface . . . . .	30
5.5	Bed boundary . . . . .	30
5.5.1	Bed concentration function . . . . .	31
5.5.2	Sediment flux function . . . . .	32
<b>6</b>	<b>Bed level changes . . . . .</b>	<b>34</b>
6.1	Equations . . . . .	34
6.2	Suspended load transport . . . . .	34
6.3	Bed-load transport . . . . .	35
6.3.1	Gradually varying flows with waves . . . . .	35
6.3.2	Complicated flows . . . . .	36
<b>7</b>	<b>Numerical solution methods and accuracy . . . . .</b>	<b>37</b>
7.1	Continuity equation for local suspended sediment . . . . .	37
7.2	Bed level changes . . . . .	38
<b>8</b>	<b>Streamline refraction for channels and trenches oblique to the flow . . . . .</b>	<b>39</b>
<b>9</b>	<b>Sensitivity analysis of controlling parameters of SUTRENCH-model . . . . .</b>	<b>41</b>
9.1	Introduction . . . . .	41
9.2	Influence of hydraulic conditions at the inlet . . . . .	41
9.3	Influence of streamline refraction . . . . .	43
9.4	Influence of particle fall velocity of suspended sediment . . . . .	45
9.5	Influence of other parameters . . . . .	46

<b>10</b>	<b>Verification of SUTRENCH-model . . . . .</b>	<b>47</b>
10.1	Introduction . . . . .	47
10.2	Migration of a channel in a flume . . . . .	47
10.3	Sedimentation in a trial dredge channel in the Western Scheldt, The Netherlands . . . . .	48
10.4	Sedimentation in a tunnel trench in a tidal river near Rotterdam, The Netherlands . . . . .	51
10.5	Sedimentation in a trial dredge channel in Asan Bay, Korea . . . . .	52
<b>11</b>	<b>Sediment trapping efficiency of dredged channels and trenches . . . . .</b>	<b>55</b>
11.1	Introduction . . . . .	55
11.2	Computations . . . . .	56
11.3	Results . . . . .	56
<b>12</b>	<b>References . . . . .</b>	<b>59</b>

## Symbols

A	coefficient	(-)
a	reference level or bed-boundary level	(L)
$\hat{a}$	amplitude of orbital excursion	(L)
b	width	(L)
C	Chézy coefficient	( $L^{0.5}S^{-1}$ )
c	concentration	( $ML^{-3}$ )
$c_a$	concentration at reference level	( $ML^{-3}$ )
$\bar{c}$	depth-averaged concentration	( $ML^{-3}$ )
D	sedimentation rate	( $ML^{-1}T^{-1}$ )
$D_a$	downward sediment transport at reference level	( $MT^{-1}L^{-2}$ )
$D_*$	particle size parameter	(-)
$d_{50}$	median particle size	(L)
d	channel depth	(L)
E	dissipation rate of turbulence energy	( $L^2T^{-3}$ )
$E_a$	upward sediment flux at reference level	( $MT^{-1}L^{-2}$ )
e	sediment trapping efficiency of dredged channels	(-)
g	acceleration of gravity	( $LT^{-2}$ )
H	wave height	(L)
$H_s$	significant wave height	(L)
h	water depth	(L)
K	turbulence energy	( $L^2T^{-2}$ )
$k_s$	equivalent or effective bed roughness height	(L)
L	length	(L)
$L_s$	significant wave length	(L)
N	number of time steps	(-)
n	number of vertical grid points	(-)
$\bar{P}$	mean static fluid pressure	( $ML^{-1}T^{-2}$ )
p	porosity factor	(-)
Q	discharge	( $ML^{-3}$ )
S	cross-section integrated sediment transport (volume)	( $L^3T^{-1}$ )
s	depth-integrated sediment transport (volume)	( $L^2T^{-1}$ )
T	bed-shear stress parameter	(-)
$T_m$	momentaneous value of bed-shear stress parameter	(-)
$T_s$	significant wave period	(T)
t	time	(T)

$u$	local flow velocity in longitudinal (x) direction	$(L T^{-1})$
$\bar{u}$	cross-section averaged flow velocity	$(L T^{-1})$
$\hat{u}$	amplitude of orbital velocity	$(L T^{-1})$
$u_*$	bed-shear velocity	$(L T^{-1})$
$u_h$	flow velocity at water surface	$(L T^{-1})$
$u_m$	flow velocity at mid depth	$(L T^{-1})$
$\bar{v}_R$	cross-section averaged flow velocity in flow direction	$(L T^{-1})$
$w$	local flow velocity in vertical (z) direction	$(L T^{-1})$
$w_s$	particle fall velocity	$(L T^{-1})$
$x$	longitudinal coordinate	$(L)$
$z$	vertical coordinate	$(L)$
$z_0$	zero-velocity level	$(L)$
$z_b$	bed level above a horizontal datum	$(L)$
$\alpha$	coefficient	$(-)$
$\alpha_0$	angle of approaching current with channel axis	$(-)$
$\beta$	ratio of sediment and fluid mixing coefficient	$(-)$
$\gamma_s$	smoothing coefficient	$(-)$
$\gamma$	angle of channel side slope	$(-)$
$\delta$	thickness of mixing layer near bed (for waves)	$(L)$
$\Delta$	relative density (under water)	$(-)$
$\Delta t$	time step	$(T)$
$\Delta x$	space step in longitudinal direction	$(L)$
$\Delta z$	space step in vertical direction	$(L)$
$\epsilon_f$	fluid mixing coefficient	$(L^2 T^{-1})$
$\epsilon_s$	sediment mixing coefficient	$(L^2 T^{-1})$
$\eta$	coefficient	$(-)$
$\kappa$	constant of Von Karman	$(-)$
$\nu$	kinematic viscosity coefficient	$(L^2 T^{-1})$
$\rho$	density	$(M L^{-3})$
$\sigma$	standard deviation of bed shear stress	$(M L^{-1} T^{-2})$
$\bar{\tau}_b$	time-averaged bed-shear stress	$(M L^{-1} T^{-2})$
$\bar{\tau}'_b$	time-averaged effective bed-shear stress	$(M L^{-1} T^{-2})$
$\phi$	turbulence-damping factor	$(-)$

## Subscripts

a	at reference level
b	bed, bottom
br	breaking conditions for waves
c	current
cw	current and waves
cr	critical
e	equilibrium conditions
f	fluid
h	at water surface
m	at mid depth
max	maximum value
R	resulting, relative
s	suspended, sediment, significant
t	total
w	wave
0	at inlet boundary ( $x = 0$ )

# 1 Introduction

The construction of a tunnel or a pipeline or a new harbour generally requires the dredging of a channel or trench in a river or estuary. Depending on the geometry of the channel, various morphological problems may arise such as sedimentation and erosion of the channel bed, local erosion near the head of the tunnelements placed in the channel and local instability of the side slopes of the channel.

Especially of importance for the client as well as the contractor are the morphological changes of the channel bed, which are caused by a local change of the flow velocity and hence the sediment transport capacity resulting in sedimentation in the deceleration zone and erosion in the acceleration zone of the channel.

As a result of serious sedimentation problems which did occur in some large tunnel trenches dredged in the years 1960 to 1970 in the Netherlands, the Dutch Office for Public Works (Rijkswaterstaat) has requested the Delft Hydraulics Laboratory to develop a mathematical model for sedimentation predictions. The purpose of such a model should be the estimation of the sedimentation in relation to the channel geometry. This study, which started in 1972 within the framework of the applied research programme of the Rijkswaterstaat, resulted in a two-dimensional vertical mathematical model for suspended sediment (SUTRENCH-model), as reported by the Delft Hydraulics Laboratory (1975), (1977), (1980a), (1980b), by Kerssens, Prins and Van Rijn, (1979) and by Van Rijn (1980, 1984).

In Chapters 2, 3, 4, 5, 6, and 7 of the present communications report a detailed description of the SUTRENCH-model is given. In chapter 8 the flow field in a channel oblique to the flow is described. In Chapter 9 the influence of the most important hydraulic parameters on the predicted sedimentation rates is shown. Finally, an extensive verification analysis concerning flume experiments and field studies is given (pipe line channel in the Western Scheldt Estuary, the Netherlands; tunnel trench near Rotterdam; navigation channel near Korea).

Futural developments will be focussed on quasi-three dimensional modelling of the suspended sediment transport to deal with converging, diverging and reversing flows.

## 2 Basic equations and simplifications for local suspended sediment

### 2.1 Continuity equation for constant width

The basic equation for the sediment continuity of the time-averaged variables in the two-dimensional (vertical) plane reads, as follows (van Rijn, 1984):

$$\frac{\partial c}{\partial t} + \frac{\partial}{\partial x}(uc) - \frac{\partial}{\partial x}\left(\varepsilon_{s,cw} \frac{\partial c}{\partial x}\right) + \frac{\partial}{\partial z}((w - w_s)c) - \frac{\partial}{\partial z}\left(\varepsilon_{s,cw} \frac{\partial c}{\partial z}\right) = 0 \quad (2.1)$$

in which:

$c$	= mean local concentration	$(kg/m^3)$
$u$	= mean local flow velocity in x-direction	$(m/s)$
$w$	= mean local flow velocity in z-direction	$(m/s)$
$w_s$	= particle fall velocity	$(m/s)$
$\varepsilon_{s,cw}$	= $\varepsilon_{s,c} + \varepsilon_{s,w}$ = sediment mixing coefficient for combined current and wave conditions	$(m^2/s)$
$\varepsilon_{s,c}$	= current – related sediment mixing coefficient	$(m^2/s)$
$\varepsilon_{s,w}$	= wave –related sediment mixing coefficient	$(m^2/s)$
$x$	= longitudinal coordinate	$(m)$
$z$	= vertical coordinate	$(m)$

Assuming steady state conditions and neglecting the longitudinal diffusive transport, which usually is an order of magnitude smaller than the other transport terms (van Rijn, 1984), Equation (2.1) reduces to:

$$\frac{\partial}{\partial x}(uc) + \frac{\partial}{\partial z}((w - w_s)c) - \frac{\partial}{\partial z}\left(\varepsilon_{s,cw} \frac{\partial c}{\partial z}\right) = 0 \quad (2.2)$$

Equation (2.2) can be solved numerically when the flow velocity, the sediment mixing coefficient, the particle fall velocity (assumed to be a constant parameter), the geometrical and physical boundary conditions are known.

For equilibrium conditions  $\left(\frac{\partial u}{\partial x} = 0, \frac{\partial w}{\partial z} = 0, \frac{\partial c}{\partial x} = 0\right)$  Equation (2.2) reduces to

$$c w_s + \varepsilon_{s,cw} \frac{\partial c}{\partial z} = 0 \quad (2.3)$$

## 2.2 Continuity equation for varying width

Assuming the local flow velocity and the local sediment concentration to be constant in lateral (y) direction, the suspended sediment transport in a laterally diverging or converging flow can be represented (to some extent) by introducing the width (b) of the flow. A laterally varying flow may either be a laterally-bounded channel with a varying width (river) or a streamtube with a varying width in a two-dimensional horizontal flow field. Integration of Equation (2.2) over the width, yields:

$$\frac{\partial}{\partial x} (buc) + \frac{\partial}{\partial z} (b(w - w_s)c) - \frac{\partial}{\partial z} \left( b \varepsilon_{s,cw} \frac{\partial c}{\partial z} \right) = 0 \quad (2.4)$$

Equation (2.4) is the basic equation of the SUTRENCH-model.

The width of the channel or streamtube must be known a priori (field or model measurements, or mathematical model results).

### 3 Flow velocity profiles

#### 3.1 Introduction

To solve Equation (2.4), the flow velocity profiles along the traject must be known. Various mathematical models can be applied to describe the flow velocity profiles, depending on the degree of perturbation of the flow (large or small bed level gradients).

For *complicated flows* including those with flow reversal (steep sided channels), a refined mathematical approach is of essential importance. A good representation of the velocity profiles can be obtained by using a K-Epsilon model, which is the most universal and widely used model for complicated flows (Rodi, 1980; Alfrink and van Rijn, 1983; van Rijn 1983b).

For long-term morphological computations, however, the K-Epsilon model is not attractive because of excessive computation costs. Therefore, a more simple model based on flexible velocity profiles and simple first order differential equations was developed (PROFILE-model). A fundamental drawback of this latter model is the need for empirical data over a wide range of conditions to calibrate the applied coefficients. When calibrated properly, however, the PROFILE-model is a powerful method for the engineering practice (reasonable results for low costs).

For *gradually varying flows* the application of a sophisticated mathematical model is not very efficient because the velocity profiles will be almost equal to those in a horizontal uniform flow. These conditions can be represented sufficiently accurately by logarithmic velocity profiles.

Since the flow conditions in practice may differ widely depending on the bed level gradients, two versions of the SUTRENCH-model have been developed:

- model for complicated flows without waves,
- model for gradually varying flows with waves.

#### 3.2 Velocity profiles for complicated flows (PROFILE model)

Since the application of a K-Epsilon model for longterm morphological computations is not very attractive because of excessive computation costs, a more simple flow

model based on the application of flexible velocity profiles as suggested by Coles (1965), was developed. A major disadvantage of this approach is the need for empirical data over a wide range of hydraulic conditions to calibrate the velocity profiles. However, when calibrated properly, the PROFILE-model is a very powerful method to compute the velocity profiles of complicated flows including those with flow reversal. The PROFILE-model is the basic method of the SUTRENCH-model to compute the velocity profiles.

### 3.2.1 Longitudinal flow velocity

Coles (1965) showed that the velocity profiles in a non-uniform flow can be described by a linear combination of a logarithmic profile representing the law of the wall and a perturbation profile representing the influence of pressure gradients. In the present study a similar approach has been used. The velocity profile is described by (see also Figure 1):

$$u = A_1 u_h \ln\left(\frac{z}{z_0}\right) + A_2 u_h F\left(\frac{z}{h}\right) \quad (3.1)$$

in which

$u$	= flow velocity at height $z$ above bed	(m/s)
$u_h$	= flow velocity at water surface ( $z = h$ )	(m/s)
$z_0$	= zero-velocity level ( $z_0 = 0.03 k_s$ )	(m)
$k_s$	= effective bed roughness	(m)
$h$	= water depth	(m)
$A_1$	= dimensionless variable	(-)
$A_2$	= dimensionless variable	(-)

The perturbation-profile  $F\left(\frac{z}{h}\right)$  is represented by:

$$F\left(\frac{z}{h}\right) = 2\left(\frac{z-z_0}{h-z_0}\right)^t - \left(\frac{z-z_0}{h-z_0}\right)^{2t} \quad (3.2)$$

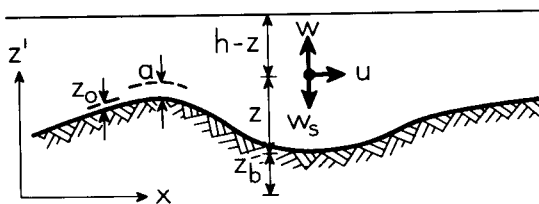


Figure 1 Definition sketch.

The  $A_2$  - variable can be determined by applying the boundary condition,  $u = u_h$  for  $z = h$  resulting in:

$$A_2 = 1 - A_1 \ln\left(\frac{h}{z_0}\right) \quad (3.3)$$

Combining Equations (3.1) (3.2) and (3.3) yields

$$u = A_1 u_h \ln\left(\frac{z}{z_0}\right) + u_h \left[1 - A_1 \ln\left(\frac{h}{z_0}\right)\right] \left[2 \left(\frac{z-z_0}{h-z_0}\right)^t - \left(\frac{z-z_0}{h-z_0}\right)\right]^{2t} \quad (3.4)$$

The flow velocity profile, as described by Equation (3.4), is completely defined when the unknown variables  $A_1$ ,  $t$  and  $u_h$  are specified. Therefore, three additional equations must be specified, which are:

- equation of continuity,
- equation for the  $t$ -parameter,
- equation for the surface flow velocity ( $u_h$ ).

#### CONTINUITY

The width-integrated discharge can be represented by:

$$Q = b \int_{z_0}^h u dz \quad (3.5)$$

in which:

$$\begin{aligned} Q &= \text{discharge} && (m^3/s) \\ b &= \text{width} && (m) \end{aligned}$$

Substitution of Equation 3.4 in Equation 3.5 and integration yields:

$$\begin{aligned} Q &= A_1 \left[ -1 + \ln\left(\frac{h}{z_0}\right) \right] b h u_h \\ &+ \left[ 1 - A_1 \ln\left(\frac{h}{z_0}\right) \right] \left[ \frac{3t+1}{2t^2+3t+1} \right] b h u_h \end{aligned} \quad (3.6)$$

#### t-PARAMETER

Analysis of flow velocity profiles measured in a channel perpendicular to the flow direction (Delft Hydraulics Laboratory, 1980a) showed that the mid-depth velocity at each location is approximately equal to the mid-depth velocity of a uniform (equilibrium) flow with the same flow velocity and water depth at that location.

Thus:

$$u_{mid-depth} = u_{mid-depth, equilibrium} \quad (3.7)$$

The mid-depth velocity is assumed to be described by Equation (3.4) resulting in:

$$u_m = A_1 u_h \ln \left( \frac{0.5h}{z_0} \right) + u_h \left[ 1 - A_1 \ln \left( \frac{h}{z_0} \right) \right] \left[ 2(0.5)^t - (0.5)^{2t} \right] \quad (3.8)$$

The mid-depth velocity for an equilibrium flow can be described by (see paragraph 3.3.1):

$$u_{m,e} = \frac{1n \left( \frac{0.5h}{z_0} \right)}{-1 + 1n \left( \frac{h}{z_0} \right)} \frac{Q}{b h} \quad (3.9)$$

Combining equations (3.7), (3.8) and (3.9), it follows that:

$$\frac{-1 + \ln \left( \frac{h}{z_0} \right)}{\ln \left( \frac{0.5h}{z_0} \right)} = \frac{3t + 1}{[2t^2 + 3t + 1][2(0.5)^t - (0.5)^{2t}]} \simeq 0.16t^2 - 0.29t + 1.02 \quad (3.10)$$

Figure 2 shows some velocity profiles according to Equations (3.6) and (3.10) for a given  $Q$ ,  $b$ ,  $h$  and  $u_h$  indicating that the method is capable of representing a wide range of velocity profiles including those with flow reversal.

#### SURFACE VELOCITY

The spatial variation of the water surface velocity is described by a simple first order differential equation which yields an exponential adjustment of the surface velocity to the equilibrium surface velocity ( $u_{h,e}$ ), as follows:

$$\frac{du_h}{dx} = \alpha_1 \frac{u_{h,e}}{h} - \alpha_2 \frac{u_h}{h} - \alpha_3 \frac{u_h}{b} \quad (3.11)$$

in which:

- $u_{h,e}$  = surface velocity for equilibrium flow (Equation (3.21)), (m/s)  
 $h$  = water depth (m)  
 $b$  = flow width (m)  
 $\alpha_1, \alpha_2, \alpha_3$  = empirical (calibration) coefficients (-)

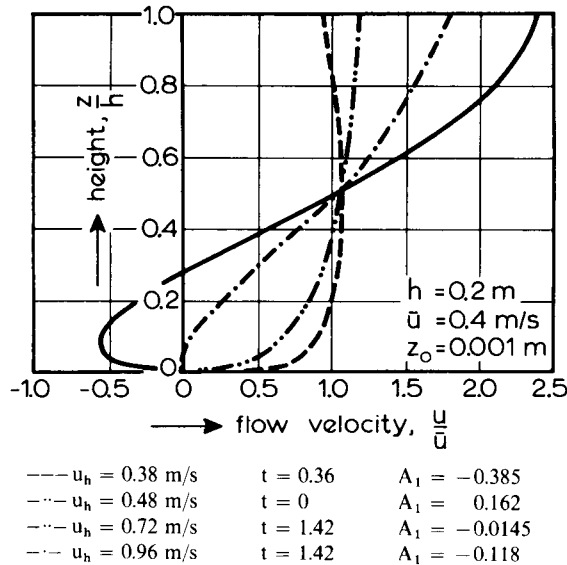


Figure 2 Velocity profiles according to PROFILE-model.

### 3.2.2 Computation procedure

Equation (3.11) can be solved numerically by using a simple Runge-Kutta method. The surface velocity at the inlet ( $u_{h,0}$ ) must be known.

The complete set of Equations (3.6), (3.10) and (3.11) is now defined and can be solved to determine the  $A_1$ ,  $t$  and  $u_h$  variables. Using Equation (3.4) the velocity profiles can be computed at each location.

The input data for the PROFILE-model are: discharge ( $Q$ ), width ( $b$ ) and depth ( $h$ ) along the trajectory, effective bed-roughness ( $k_s$ ), Constant of Von Karman ( $\kappa$ ) and the surface velocity ( $u_{h,0}$ ) at the inlet.

### 3.2.3 Calibration

The coefficients which have to be calibrated are the  $\alpha_1$ ,  $\alpha_2$  and  $\alpha_3$  – coefficients of Equation (3.11). For that purpose measured velocity profiles in a channel

perpendicular to the flow direction were used (Delft Hydraulics Laboratory, 1980a). Seven experiments with various channel geometries and hydraulic conditions (T1, T6, T7, T8, T13, T14 and T16) were selected. Based on fitting of measured and computed velocity profiles the  $\alpha_1$  and  $\alpha_2$  - coefficients were found to be dependent on the local bottom slope ( $dh/dx$ ), as follows:

$$\alpha_1 = 0.28 + 0.11 \tanh [6(dh/dx) - 0.15] \tag{3.12}$$

$$\alpha_2 = 0.235 + 0.065 \tanh [17(dh/dx) - 0.035] \tag{3.13}$$

The  $\alpha_3$ -coefficient represents the adjustment of the surface velocity to lateral (width) variations. Since experimental data were not available, the  $\alpha_3$ -coefficient could not be calibrated. Therefore, an expression is applied which yields a gradual adjustment of the surface velocity, as follows:

$$\alpha_3 = 0.1 \tanh [10(db/dx)] \tag{3.14}$$

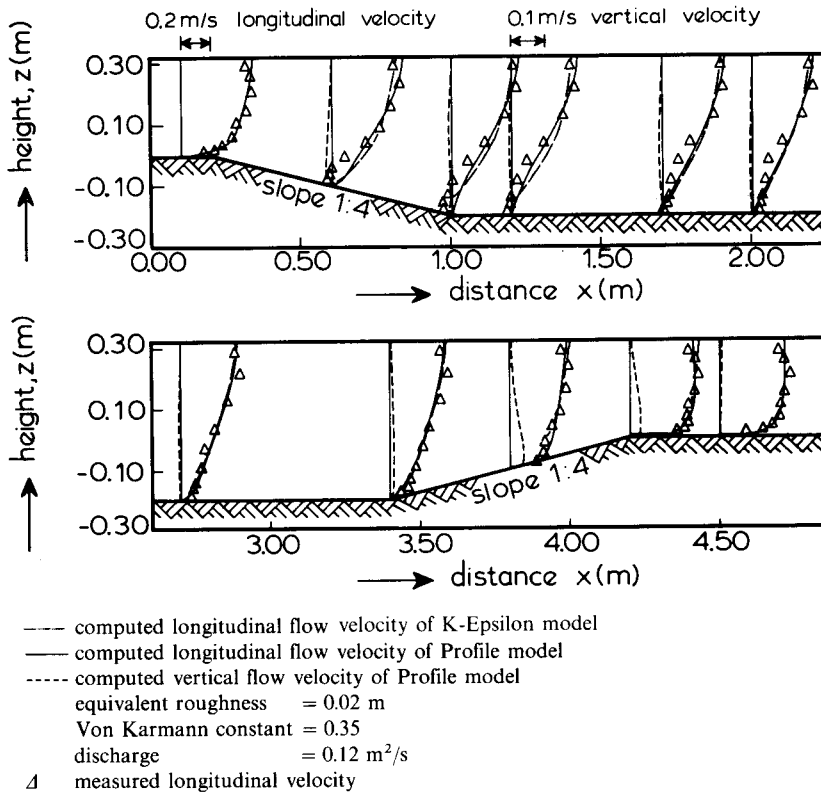


Figure 3 Measured and computed velocity profiles in a channel perpendicular to the flow.

Figure 3 shows computed and measured velocity profiles in a channel perpendicular to the flow (T14). The agreement between measured and computed velocity profiles is reasonably good in the acceleration zone but less good in the deceleration zone of the channel. The results of a K-Epsilon model are also shown. The results of the PROFILE-model and the sophisticated K-Epsilon model show similar deviations compared with the measured values.

Finally, it may be noted that the experimental results show serious three-dimensional effects, particularly in the deceleration zone. This is indicated by the specific discharge (per unit width) in the centre line of the flume, which is relatively small in the deceleration zone compared with the value at the inlet.

### 3.2.4 Vertical flow velocity

Applying the (width-integrated) equation of continuity for the fluid:

$$\frac{1}{b} \frac{\partial(bu)}{\partial x} + \frac{\partial w}{\partial z} = 0 \quad (3.15)$$

the vertical flow velocity ( $w$ ) can be computed as (see Figure 1):

$$w = - \int_{z_b+z_0}^{z_b+z} \frac{\partial u}{\partial x} dz - \frac{1}{b} \frac{db}{dx} \int_{z_b+z_0}^{z_b+z} u dz \quad (3.16)$$

Substitution of Equation (3.4) and integration yields a (complicated) analytical expression for the vertical flow velocity.

### 3.2.5 Bed-shear velocity

The bed-shear velocity ( $u_*$ ) is determined from the flow velocity computed at a height  $z = 0.05 h$  above the bed assuming a logarithmic profile in the near-bed layer ( $z < 0.05 h$ ) as follows:

$$u_* = \frac{\kappa u_b}{1n \left( \frac{0.05 h}{z_0} \right)} \quad (3.17)$$

in which:

$u_b$	= flow velocity at $z = 0.05 h$ above mean bed	(m/s)
$\kappa$	= Constant of Von Karman	(-)
$h$	= water depth	(m)
$z_0$	= zero-velocity level (= $0.03 k_s$ )	(m)

### 3.3 Velocity profiles for gradually varying flows with waves

For gradually varying flow conditions (say  $dh/dx \leq 0.05$  and  $db/dx \leq 0.05$ ) the application of a sophisticated method to compute the velocity profiles is not very efficient because the velocity profiles will almost be equal to those for a uniform (equilibrium) flow. It is assumed that for these conditions the velocity profiles can be represented sufficiently accurately by simple logarithmic profiles. The influence of the waves on the (time-averaged) velocities is not represented in the present study.

#### 3.3.1 Longitudinal flow velocity

The logarithmic velocity profile is represented by:

$$u = A_1 u_{h,e} \ln\left(\frac{z}{z_0}\right) \quad (3.18)$$

in which:

$A_1$	= roughness parameter	(-)
$u_{h,e}$	= surface velocity for an equilibrium flow	(m/s)
$z_0$	= zero-velocity level (= $0.03 k_s$ )	(m)
$k_s$	= current-related bed-roughness	(m)

Applying the boundary condition:  $u = u_h$  at  $z = h$ , it follows that:

$$A_1 = \frac{1}{\ln\left(\frac{h}{z_0}\right)} \quad (3.19)$$

Substitution of Equation (3.18) in the continuity Equation (3.5) and integration yields:

$$Q = b \int_{z_0}^h u dz = A_1 b h u_{h,e} \left[ -1 + \ln\left(\frac{h}{z_0}\right) \right] \quad (3.20)$$

Substitution of Equation (3.19) in Equation (3.20) yields:

$$u_{h,e} = \frac{\ln\left(\frac{h}{z_0}\right)}{-1 + \ln\left(\frac{h}{z_0}\right)} \frac{Q}{b h} \quad (3.21)$$

The bed-shear velocity follows from:

$$A_1 u_{h,e} = \frac{u_{*,e}}{\kappa} \quad (3.22)$$

resulting in:

$$u_{*,e} = A_1 \kappa u_{h,e} = \frac{\kappa}{-1 + \ln\left(\frac{h}{z_0}\right)} \frac{Q}{bh} \quad (3.23)$$

Equation (3.23) yields similar results as the following (well-known) expression:

$$u_{*,e} = \frac{g^{0.5}}{C} \frac{Q}{bh} \quad (3.24)$$

in which:

$g$  = acceleration of gravity (m/s<sup>2</sup>)

$C = 18 \log\left(\frac{12h}{k_s}\right)$  = Chèzy coefficient (m<sup>0.5</sup>/s)

### 3.3.2 Vertical flow velocity

Applying the width-integrated equation of continuity:

$$\frac{1}{b} \frac{\partial(bu)}{\partial x} + \frac{\partial w}{\partial z} = 0 \quad (3.25)$$

the vertical flow velocity can be computed as:

$$w = - \int_{z_b+z_0}^{z_b+z} \frac{\partial u}{\partial x} dz - \frac{1}{b} \frac{db}{dx} \int_{z_b+z_0}^{z_b+z} u dz \quad (3.26)$$

Combining Equation (3.18) and (3.26) it follows that:

$$\begin{aligned} w = & \left[ z - z_1 n \left( \frac{z}{z_0} \right) \right] \left[ A_1 \frac{du_{h,e}}{dx} + u_{h,e} \frac{dA_1}{dx} \right] - A_1 u_{h,e} n \left( \frac{z}{z_0} \right) \frac{dh}{dx} \\ & + \frac{A_1 u_{h,e}}{b} \left[ z - h - z_1 n \left( \frac{z}{z_0} \right) + h n \left( \frac{h}{z_0} \right) \right] \frac{db}{dx} - \frac{Q}{b^2} \frac{db}{dx} \end{aligned} \quad (3.27)$$

in which :

$$\frac{du_{h,e}}{dx} = \frac{\left[ \bar{u} \frac{dh}{h dx} + 1n \left( \frac{h}{z_0} \right) \frac{d\bar{u}}{dx} \right] \left[ -1 + 1n \left( \frac{h}{z_0} \right) \right] - \left[ \frac{u 1n \left( \frac{h}{z_0} \right)}{h} \right] \frac{dh}{dx}}{\left[ -1 + 1n \left( \frac{h}{z_0} \right) \right]^2} \quad (3.28)$$

$$\frac{dA_1}{dx} = - \frac{1}{h \left[ 1n \left( \frac{h}{z_0} \right) \right]^2} \frac{dh}{dx} \quad (3.29)$$

$$\frac{d\bar{u}}{dx} = \left[ - \frac{1}{bh^2} \frac{dh}{dx} - \frac{1}{b^2 h} \frac{db}{dx} \right] Q \quad (3.30)$$

$$\bar{u} = \frac{Q}{bh} \quad (3.31)$$

In case of a varying width but a uniform depth ( $dh/dx = 0$ ) Equation (3.27) yields a zero vertical velocity.

## 4 Fluid and sediment mixing coefficient

### 4.1 Introduction

The sediment mixing coefficient is related to the fluid mixing coefficient as follows:

$$\varepsilon_s = \beta \phi \varepsilon_f \quad (4.1)$$

in which:

$\varepsilon_s$	= sediment mixing coefficient	(m <sup>2</sup> /s)
$\varepsilon_f$	= fluid mixing coefficient	(m <sup>2</sup> /s)
$\beta$	= ratio sediment mass mixing and fluid momentum mixing coefficients	(-)
$\phi$	= turbulence damping factor	(-)

The  $\beta$ -factor represents the difference in the diffusion (or mixing) of a fluid 'particle' (or small coherent fluid structure) and a discrete sediment particle and is assumed to be constant over the water depth. Based on experimental data of Coleman (1970), the  $\beta$ -factor was found to be in the range 1 to 3 (van Rijn, 1982a). The  $\phi$ -factor expresses the damping of the turbulence by the sediment particles resulting in a reduction of the fluid mixing coefficient. This effect was studied by van Rijn (1982 a). For concentrations smaller than 10.000 mg/l the influence of the  $\phi$ -factor is relatively small and may, therefore, be neglected for most practical cases.

### 4.2 Mixing coefficients for complicated flows (PROFILE-model)

Since the computation of the fluid mixing coefficient by a sophisticated mathematical model (K-Epsilon turbulence model) is not attractive for long-term morphological computations because of excessive computation time, a more simple method based on the application of flexible profiles was developed. Fluid mixing coefficients computed by a K-Epsilon turbulence model for a limited set of hydraulic conditions were used for calibration of the simple profile-method.

#### 4.2.1 Vertical distribution of fluid mixing coefficient

In vertical direction a parabolic-constant profile is used which means a constant

(maximum) value in the upper half of the depth and a parabolic distribution in the lower half of the depth, as follows (see Figure 4):

$$\varepsilon_f = \varepsilon_{f,max} - \varepsilon_{f,max} \left(1 - \frac{2z}{h}\right)^2 \quad \text{for } \frac{z}{h} < 0.5 \quad (4.2a)$$

$$\varepsilon_f = \varepsilon_{f,max} \quad \text{for } \frac{z}{h} \geq 0.5 \quad (4.2b)$$

$$\varepsilon_s = \beta \varepsilon_f \quad (4.2c)$$

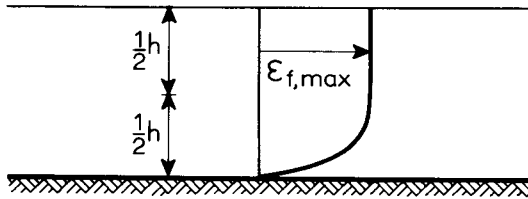


Figure 4 Vertical distribution of fluid mixing coefficient.

The reason for applying a constant  $\varepsilon_f$ -value in the upper half of the depth is that it yields a finite concentration at the water surface and more realistic concentrations in the upper part of the depth (van Rijn, 1982 a). The parabolic-constant distribution was introduced by Kerssens (1977).

#### 4.2.2 Longitudinal distribution of fluid mixing coefficient

The variation of the mixing coefficients in longitudinal direction is effectuated by varying the  $\varepsilon_{f,max}$ -value applying a simple first order differential equation, as follows:

$$\frac{d\varepsilon_{f,max}}{dx} = \left[ \frac{\alpha_4}{h} (\varepsilon_{f,max,e} - \varepsilon_{f,max}) - \alpha_5 h \frac{d(u_h - \bar{u})}{dx} \right] e^{-1.5 dh/dx} \quad (4.3)$$

in which:

- $\varepsilon_{f,max,e} = 0.25 \kappa u_{*,e} h$  = maximum fluid mixing coefficient for equilibrium (uniform) conditions (m<sup>2</sup>/s)
- $u_h$  = surface velocity according to Equation (3.11) (m/s)
- $\bar{u}$  = cross-section averaged velocity (m/s)

- $u_{*,e}$  = bed-shear velocity for equilibrium conditions (m/s)  
 according to Equation (3.23)  
 $\kappa$  = Constant of Von Karman (-)  
 $h$  = water depth (-)  
 $\alpha_4, \alpha_5$  = empirical coefficients (-)

Term I represents the decrease of the  $\epsilon_{f,max}$ -value towards its equilibrium value. Term II represents the increase of the  $\epsilon_{f,max}$ -value after a change of the flow velocity profile. Term III is a stabilizing term acting at steep sloping bottoms. Equation (4.3) can be solved numerically for a given  $\epsilon_{f,max}$ -value at the inlet ( $x = 0$ ).

### 4.2.3 Calibration

The  $\alpha_4$ - and  $\alpha_5$ -coefficients were determined by calibration using mixing coefficient distributions computed by the K-Epsilon model for various channel geometries, yielding:

$$\alpha_4 = 0.05$$

$$\alpha_5 = 0.015$$

Figure 5 shows some calibration results for a channel perpendicular to the flow. Generally, the values of the K-Epsilon model are somewhat smaller in the upper half of the depth and somewhat larger in the lower half of the depth, particularly in the acceleration zone. These deviations donot seriously influence the predicted sedimentation rates of dredged channels (van Rijn, 1984).

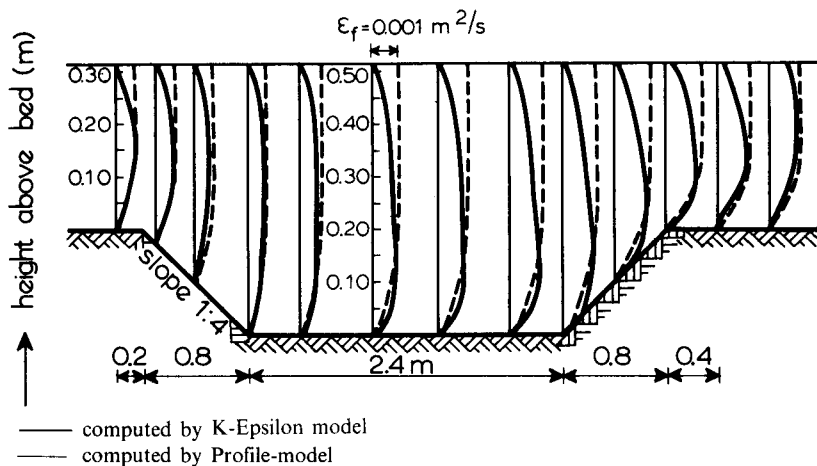


Figure 5 Computed fluid mixing coefficients for a channel perpendicular to the flow

### 4.3 Mixing coefficients for gradually varying flows with waves

In case of a gradually varying flow ( $dh/dx < 0.05$ ,  $db/dx < 0.05$ ) it is assumed to be acceptable to use simple mixing coefficient distributions, as used for equilibrium (uniform) conditions.

#### 4.3.1 Current alone

For equilibrium conditions the sediment mixing coefficient usually is represented by a parabolic distribution:

$$\varepsilon_{s,c} = \beta \kappa u_{*,c} z \left(1 - \frac{z}{h}\right) \quad (4.4)$$

in which:

$$u_{*,c} = \text{bed-shear velocity for a current alone according to Equation (3.23)} \quad (\text{m/s})$$

Equation (4.4) yields a zero-concentration at the water surface, which is not very realistic. Therefore, in the present study a parabolic-constant mixing coefficient distribution, introduced by Kerssens (1977), is applied:

$$\varepsilon_{s,c} = \varepsilon_{s,c,max} - \varepsilon_{s,c,max} \left(1 - \frac{2z}{h}\right)^2 \quad \text{for } \frac{z}{h} < 0.5 \quad (4.5a)$$

$$\varepsilon_{s,c} = \varepsilon_{s,c,max} = 0.25 \beta \kappa u_{*,c} h \quad \text{for } \frac{z}{h} \geq 0.5 \quad (4.5b)$$

Equation (4.5) is shown in Figure 6.

The  $\varepsilon_{s,c,max}$ -value is equal to the maximum value of the parabolic distribution according to Equation (4.4).

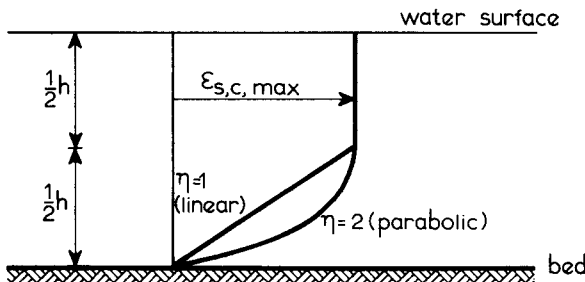


Figure 6 Current-related mixing coefficients.

### 4.3.2 Waves alone

Based on the analysis of concentration profiles generated by waves, the wave-related sediment mixing coefficient was found to be (van Rijn, 1985):

$$\varepsilon_{s,w} = \varepsilon_{s,w,bed} \quad , \text{ for } z \leq \delta \quad (4.6a)$$

$$\varepsilon_{s,w} = \varepsilon_{s,w,max} \quad , \text{ for } z \geq 0.5h \quad (4.6b)$$

$$\varepsilon_{s,w} = \varepsilon_{s,w,bed} + (\varepsilon_{s,w,max} - \varepsilon_{s,w,bed}) \left( \frac{z - \delta}{0.5h - \delta} \right) \quad , \text{ for } \delta < z < 0.5h \quad (4.6c)$$

in which:

$\varepsilon_{s,w,bed}$  = wave-related sediment mixing coefficient close to the bed (m<sup>2</sup>/s)

$\varepsilon_{s,w,max}$  = wave-related sediment mixing coefficient in upper half of depth (m<sup>2</sup>/s)

$\delta$  = thickness of near-bed mixing layer (m)

Equation (4.6) is shown in Figure 7.

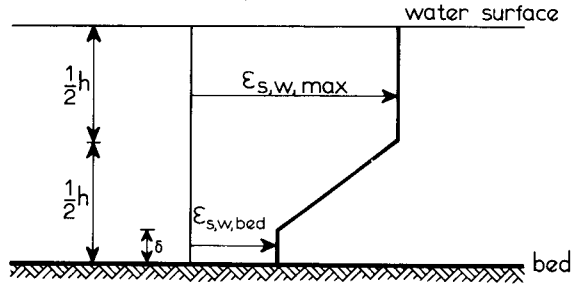


Figure 7 Wave-related sediment mixing coefficient.

Measured concentration profiles were analyzed to relate the characteristic parameters of the sediment mixing distribution to general wave parameters yielding (van Rijn, 1985):

$$\varepsilon_{s,w,bed} = 0.00065 D_*^2 \alpha_{br} \delta \hat{u}_{b,w} \quad (4.7)$$

$$\varepsilon_{s,w,max} = 0.035 \alpha_{br} \frac{h H_s}{T_s'} \quad (4.8)$$

$$\delta = 0.06 \quad (4.9)$$

in which:

$$D_* = d_{50} \left( \frac{\Delta g}{\nu^2} \right)^{1/3} = \text{particle size parameter} \quad (-) \quad (4.10)$$

$$\hat{u}_{b,w} = \frac{\pi H_s}{T_s \sinh(2\pi h/L_s)} = \text{peak value of orbital velocity at bed} \quad (\text{m/s}) \quad (4.11)$$

$\alpha_{br}$  = breaking coefficient representing the influence of breaking waves on the sediment mixing process (-)

$H_s$  = significant wave height (m)

$L_s$  = significant wave length (m)

$T'_s$  = significant wave period (relative to moving coordinate system) (s)

$\Delta$  =  $(\rho_s - \rho)/\rho$  = relative density (-)

$g$  = acceleration of gravity (m/s<sup>2</sup>)

$\nu$  = kinematic viscosity coefficient (m<sup>2</sup>/s)

The breaking coefficient ( $\alpha_{br}$ ) was found to be dependent on the relative wave height (van Rijn, 1985), as follows:

$$\alpha_{br} = 5 \left( \frac{H_s}{h} \right) - 2, \quad \text{for } \frac{H_s}{h} \geq 0.6 \text{ (breaking waves)} \quad (4.10a)$$

$$\alpha_{br} = 1, \quad \text{for } \frac{H_s}{h} < 0.6 \text{ (non-breaking waves)} \quad (4.10b)$$

### 4.3.3 Current and waves

When a wave field is superimposed on a current, the overall sediment mixing is represented by a linear addition of the wave-related and current-related mixing coefficients (van Rijn, 1985), as follows:

$$\varepsilon_{s,cw} = \varepsilon_{s,c} + \varepsilon_{s,w} \quad (4.11)$$

in which:

$\varepsilon_{s,cw}$  = sediment mixing coefficient for current and waves (m<sup>2</sup>/s)

$\varepsilon_{s,c}$  = current-related sediment mixing coefficient (m<sup>2</sup>/s)

$\varepsilon_{s,w}$  = wave-related sediment mixing coefficient (m<sup>2</sup>/s)

#### WAVE - RELATED MIXING

It is assumed that the wave-related mixing is not modified by the presence of a current. Therefore, Equation (4.6) is applied (see also Figure 7).

Because of the presence of waves, the mean current velocity profile is modified (van Rijn, 1985). Therefore, it is logical to assume that the current-related mixing is also modified. This effect has been represented by adjusting the mixing coefficient (in the lower half of the depth) of a current alone, as described by Equation (4.5), as follows:

$$\varepsilon_{s,c} = \varepsilon_{s,c,max} - \varepsilon_{s,c,max} \left(1 - \frac{2z}{h}\right)^\eta \quad \text{for } \frac{z}{h} < 0.5 \quad (4.12a)$$

$$\varepsilon_{s,c} = \varepsilon_{s,c,max} = 0.25 \beta \kappa u_{*,c} h \quad \text{for } \frac{z}{h} \geq 0.5 \quad (4.12b)$$

in which:

$$\eta = \text{coefficient} \quad (-)$$

$$u_{*,c} = \text{bed-shear velocity for equilibrium conditions} \\ \text{according to Equation (3.23)} \quad (\text{m/s})$$

The  $\varepsilon_{s,c,max}$ -value is not supposed to be modified. The  $\eta$ -coefficient is assumed to be in the range  $\eta = 1$  (linear) to  $\eta = 2$  (parabolic) depending on the relative strength of the wave motion ( $\hat{u}_{b,w}$ ) and the mean current ( $\bar{u}$ ). Equation (4.12) is shown in Figure 6.

Based on the analysis of measured concentration profiles, it was found (van Rijn, 1985):

$$\eta = -0.25 \frac{\hat{u}_{b,w}}{|\bar{u}|} + 2, \quad \text{for } 0 \leq \frac{\hat{u}_{b,w}}{|\bar{u}|} \leq 4 \quad (4.13a)$$

$$\eta = 1, \quad \text{for } \frac{\hat{u}_{b,w}}{|\bar{u}|} > 4 \quad (4.13b)$$

#### 4.4 Equilibrium concentration profiles

Applying Equation (2.3) and the proposed expressions for the mixing coefficient, a concentration profile for equilibrium conditions can be computed analytically or numerically (van Rijn, 1984).

## 5 Boundary conditions

### 5.1 Flow domain

The following specifications are required:

- Initial ( $t = 0$ ) bottom-level profiles along the traject:  $z_b = f(x, t = 0)$
- Water depth along the traject :  $h = f(x, t = 0)$
- flow width along the traject :  $b = f(x)$

The water surface is assumed to be horizontal. Water level variations due to acceleration and deceleration effects are neglected.

### 5.2 Inlet boundary

The inlet boundary should be selected at a location where no or minor morphological changes are to be expected. For unidirectional flow this location should be chosen as close as possible to the area of interest. In case of tidal flow the inlet boundary should be far away from the area of interest.

The following specifications are required:

- discharge :  $Q = f(t)$
- flow velocity distribution :  $u = f(z, t)$
- mixing coefficient distribution :  $\varepsilon_s = f(z, t)$
- sediment concentration distribution :  $c = f(z, t)$

Preferably, measured concentration profiles should be used at the inlet ( $x = 0$ ). Special cases are an equilibrium concentration profile or a zero-concentration (no initial load) profile specified at the inlet.

### 5.3 Outlet boundary

The location of the outlet boundary should always be far away from the area of interest. As the water surface is assumed to be horizontal, no additional specifications are required.

## 5.4 Water surface

The net vertical sediment transport is assumed to be zero, resulting in :

$$\left( w_s c + \varepsilon_s \frac{\partial c}{\partial z} \right)_{z = z_b + h} = 0 \quad (5.1)$$

## 5.5 Bed boundary

- flow velocity :  $w = 0$  at  $z = z_0$  (5.2)

- concentration :  $c_a$  specified at  $z = z_b + a$ , or (5.3)

$$E_a = \left( -\varepsilon_s \frac{\partial c}{\partial z} \right)_a \text{ specified at } z = z_b + a \quad (5.4)$$

The bed concentration ( $c_a$ ) as well as the upward sediment flux ( $E_a$ ) are specified by functions which relate those variables to local near-bed flow, wave and sediment parameters. The applied functions are presented in paragraphs 5.5.1 and 5.5.2.

When the flow is varying rapidly, the application of a bed-concentration type of boundary condition may result in a positive concentration gradient near the bed (see Figure 8) which is physically not realistic. In that case the concentration at that location ( $x_i$ ) is recomputed applying a zero-concentration gradient as bed-boundary condition ( $\partial c_a / \partial z = 0$ ).

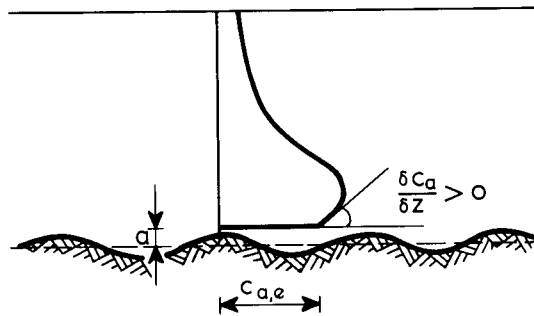


Figure 8 Positive bed-concentration gradient.

The bed-boundary condition is specified at an arbitrary level ( $a$ ) above the mean bed level. It is attractive to apply a bed-boundary level close to the bed, because in that case the bed concentration (or the flux) can be represented by their equilibrium values assuming that there is an almost instantaneous adjustment to equilibrium conditions close to the bed. Detailed experimental research has shown

that these assumptions are reasonable (Delft Hydraylic Laboratory, M1531-I, 1981a; M1531-II, 1981b; M1531-III, 1983a and M1531-IV, 1983b).

### 5.5.1 Bed concentration function

#### GRADUALLY VARYING FLOWS WITH WAVES

For these conditions a simple deterministic function, as proposed by van Rijn (1982a, 1985) for sand particles, is used. This function relates the *equilibrium* bed concentration ( $c_{a,e}$ ) to local flow, wave and sediment parameters, as follows:

$$c_{a,e} = 0.015 \frac{d_{50}}{a} \frac{T^{1.5}}{D_*^{0.3}} \quad (5.5)$$

in which:

$$D_* = d_{50} \left( \frac{\rho_s - \rho}{\rho} \frac{g}{\nu^2} \right)^{1/3} = \text{particle size parameter} \quad (-)$$

$$T = \frac{\bar{\tau}'_{b,cw} - \bar{\tau}_{b,cr}}{\bar{\tau}_{b,cr}} = \text{shear-stress parameter} \quad (-)$$

$\bar{\tau}'_{b,cw}$  = effective bed-shear stress for flows with waves  
(van Rijn, 1985) (N/m<sup>2</sup>)

$\bar{\tau}_{b,cr}$  = critical bed-shear stress for initiation of motion  
according to Shields (N/m<sup>2</sup>)

$d_{50}$  = median particle size (m)

$a$  = reference level (m)

$\rho_s$  = sediment density (kg/m<sup>3</sup>)

$\rho$  = fluid density (kg/m<sup>3</sup>)

$g$  = acceleration of gravity (m/s<sup>2</sup>)

$\nu$  = kinematic viscosity coefficient (m<sup>2</sup>/s)

Equation (5.5) specifies a dimensionless concentration. Multiplying by  $\rho_s 10^3$  yields a concentration in mg/l.

#### COMPLICATED FLOWS WITHOUT WAVES

For complicated flows where flow separation and flow reversal may occur, a deterministic approach as expressed by Equation (5.5) does not yield realistic

results. In such flows the (effective) bed-shear stress in or near the separation and reattachment point may approach zero resulting in a zero-bed concentration or flux (applying a deterministic equation), which is not realistic in a physical sense. Therefore, a stochastic approach is introduced to represent the influence of the velocity fluctuations close to the bed which have a dominating effect on the pick-up of sediment particles near the separation and reattachment points.

Applying a stochastic approach (van Rijn, 1984), the time-averaged bed concentration ( $c_a$ ) can be expressed as:

$$c_a = 0.03 \frac{d_{50}}{a} \frac{\overline{T_m^{1.5}}}{D_*^{0.3}} \quad (5.6)$$

in which:

$$\overline{T_m^{1.5}} = \frac{1}{(2\pi)^{0.5}} \left[ \left( \frac{\sigma'}{\tau_{b,cr,1}} \right)^{1.5} |J_1| + \left( \frac{\sigma'}{\tau_{b,cr,2}} \right)^{1.5} |J_2| \right] = \text{stochastic shear-stress parameter}$$

$\sigma'$  = standard deviation of effective bed-shear stress (N/m<sup>2</sup>)

$\tau_{b,cr}$  = momentaneous critical bed-shear stress (N/m<sup>2</sup>)

The  $J_1$  and  $J_2$  integrals as well as expressions for the critical bed-shear stress are given by van Rijn (1984).

### 5.5.2 Sediment flux function

Applying Equation (2.3), it follows for equilibrium conditions that:

$$E_a = -w_s c_a \quad (5.7)$$

It is assumed that the upward sediment flux at the bed in non-uniform ( $\partial\bar{u}/\partial x \neq 0$ ) conditions will be approximately equal to its equilibrium value for uniform conditions.

#### GRADUALLY VARYING FLOWS

Substitution of Equation (5.5) in Equation (5.7) yields:

$$E_a = \left( -\varepsilon_s \frac{\partial c}{\partial z} \right)_a = -0.015 w_s \frac{d_{50}}{a} \frac{T^{1.5}}{D_*^{0.3}} \quad (5.8)$$

$$E_a = \left( -\varepsilon_s \frac{\partial c}{\partial z} \right)_a = -0.03 w_s \frac{d_{50}}{a} \frac{\overline{T_m}^{1.5}}{D_*^{0.3}} \quad (5.9)$$

For hydraulic conditions below those for initiation of motion, Equations (5.8) and (5.9) yield a zero-upward sediment flux which is specified as a zero-concentration gradient ( $\partial c_a / \partial z = 0$ ).

## 6 Bed level changes

### 6.1 Equations

After computation of the concentration field the bed level changes are computed using the cross-section-integrated continuity equation, which reads as follows:

$$\frac{\partial bz_b}{\partial t} + \frac{1}{\rho_s(1-p)} \left[ \frac{\partial bh\bar{c}}{\partial t} + \frac{\partial S}{\partial x} \right] = 0 \quad (6.1)$$

in which:

$z_b$	= bed level with respect to reference datum	(m)
$t$	= time	(s)
$p$	= porosity factor	(-)
$b$	= width	(m)
$h$	= water depth	(m)

$$\bar{c} = \frac{1}{h} \int_{z_b+a}^{z_b+h} c dz = \text{depth-averaged concentration} \quad (\text{kg/m}^3)$$

$S$	$= S_s + S_b$	= cross-section integrated total load	(m <sup>3</sup> /s)
$S_s$		= cross-section integrated suspended load	(m <sup>3</sup> /s)
$S_b$		= cross-section integrated bed load	(m <sup>3</sup> /s)
$\rho_s$		= sediment density	(kg/m <sup>3</sup> )

Assuming quasi-steady flow conditions, the storage term ( $\partial bh\bar{c}/\partial t$ ) can be neglected.

### 6.2 Suspended load transport

The suspended load transport is computed as:

$$S_s = b \int_{z_b+a}^{z_b+h} u c dz \quad (6.2)$$

in which:

$c$ = local concentration	(kg/m <sup>3</sup> )
$u$ = local flow velocity	(m/s)
$a$ = reference level	(m)
$z$ = vertical coordinate	(m)

### 6.3 Bed-load transport

The transport of sediment particles below the bed-boundary level ( $z_b + z_0 < z < z_b + a$ ) is represented as bed-load transport using a simple formula. This schematization implies the selection of a bed-boundary level ( $a$ ) close to the bed. In the present study this level is assumed to be located at the top of the bed forms. Thus  $a \approx \frac{1}{2} \Delta_b$  ( $\Delta_b$  = bed-form height) with a minimum value of  $a = 0.01 h$  for reasons of accuracy (van Rijn, 1982a).

This approach requires information of the bed-form height, which can be obtained by measurements (echo soundings) or predictions (van Rijn, 1982b). Finally, it is noted that the computed bed-load transport may be rather inaccurate. This, however, does not seriously effect the overall results of the SUTRENCH-model, when the model is applied for conditions with a dominating suspended load.

#### 6.3.1 Gradually varying flows with waves

For a current alone the bed-load transport can be represented by a simple formula, as follows (van Rijn, 1982a):

$$S_b = 0.053 b (\Delta g)^{0.5} d_{50}^{1.5} \frac{T^{2.1}}{D_*^{0.3}} \quad (6.3)$$

in which:

$S_b$ = bed-load transport	(m <sup>3</sup> /s)
$\Delta = (\rho_s - \rho) / \rho$ = relative density	(-)

Gravity effects at sloping bottoms resulting in an increased bed-load transport rate at a downward sloping bottom and a reduced value at an upward sloping bottom are taken into account via the  $T$ -parameter.

In case of hydraulic conditions with currents and waves a generally accepted formula for the bed-load transport is not available. Therefore, the following approach is used:

$$S_b = a b c_a u_a \quad (6.4)$$

in which :

$a$	= thickness of bed-load layer	(m)
$b$	= flow width	(m)
$c_a$	= (volume) concentration at reference level ( $z = a$ )	(-)
$u_a$	= flow velocity at reference level ( $z = a$ )	(m/s)

The thickness of the bed-load layer is assumed to be equal to the distance between the reference level and the mean bed level. The concentrations in this layer are assumed to be constant and equal to the concentration ( $c_a$ ) computed at the reference level. It is realized that this schematization is rather crude, but since the bed-load transport is small compared with the suspended load transport possible errors do not have a significant effect on the accuracy of the total load transport.

### 6.3.2 *Complicated flows*

The bed-load transport is represented by a stochastic version of Equation (6.3), as follows (van Rijn, 1984):

$$S_b = 0.1 b (\Delta g)^{0.5} d_{50}^{1.5} \frac{\overline{T_m^{2.1}}}{D_*^{0.3}} \quad (6.5)$$

## 7 Numerical solution methods and accuracy

### 7.1 Continuity equation for local suspended sediment

To solve Equation (2.4), a finite element method based on weighted residuals according to the (modified) Galerkin-method is used.

The continuous solution (two-dimensional) domain is divided into a system of quadrangular elements. The vertical dimensions of the elements decrease towards the bed to provide a greater resolution in the zone where large velocity and concentration gradients exist. Between the nodes of the elements the unknown variable is represented by a linear function. Then, for each element the coefficients corresponding to the unknown variable at each node are determined. Finally, the (tri-diagonal) coefficients matrix for the complete solution domain is determined, from which the coefficients can be solved (Vreugdenhil, 1982). A detailed accuracy analysis shows that in vertical direction at least 10 grid points should be used for

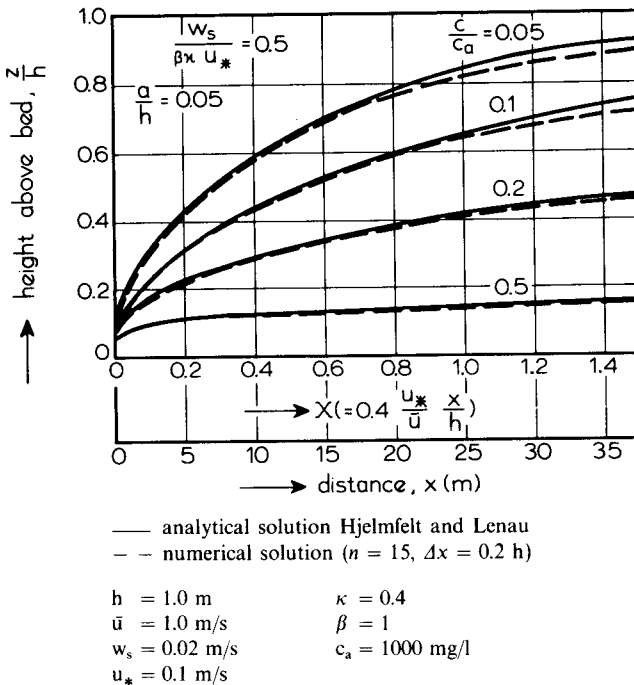


Figure 9 Comparison of analytically and numerically computed concentrations.

conditions with a current alone and at least 20 points for currents superimposed by waves. In longitudinal direction at least 10 element lengths should be used over the characteristic length scale of the bottom profile (side slope length of a dredged channel).

For a horizontally uniform flow (without waves) the results of the numerical solution method can be compared with an analytical solution. Hjelmfelt and Lenau (1970) presented an analytical solution of Equation (2.2) assuming a:

- parabolic sediment mixing coefficient (Equation (4.4)),
- constant flow velocity in vertical direction and
- constant bed concentration in longitudinal direction.

Figure 9 shows the results of the analytical solution and the (present) numerical solution for a specific case ( $w_s/\beta\kappa u_* = 0.5$ ). The numerical solution is based on 15 grid points in vertical direction,  $\Delta x = 0.2 h$  and a bed concentration specified at  $a = 0.05 h$ . The numerical inaccuracy increases towards the water surface which is caused by the variable element size in vertical direction yielding relatively large vertical element sizes near the water surface. The maximum error is about 5 to 10%, which is quite acceptable for engineering purposes.

## 7.2 Bed level changes

Bed level changes are computed from the cross-section integrated sediment transport (Equation (6.1)).

For the computation of the new bed level at time  $t + \Delta t$  from the known bed level at time  $t$  the following numerical scheme (LAX-scheme) is used:

$$z_{b,x}^{t+\Delta t} = z_{b,x}^t - \frac{N \Delta t}{2(1-p)\rho_s b \Delta x} (S_{x+\Delta x}^t - S_{x-\Delta x}^t) + \frac{1}{2}\gamma_s (z_{b,x+\Delta x}^t - 2z_{b,x}^t + z_{b,x-\Delta x}^t). \quad (7.1)$$

The  $\gamma_s$ -factor in Equation (7.1) determines to what extent the bed levels of the surrounding points of  $z_{b,x}$  are taken into account for the computation of the new bed level  $z_{b,x}$  at time  $t + \Delta t$ . This causes numerical smoothing at sharp transitions of the bed level profile. Numerical inaccuracy is minimal for a proper selection of the (numerical)  $\gamma_s$ ,  $N$  and  $\Delta t$  parameter.

## 8 Streamline refraction for channels and trenches oblique to the flow

Generally, sedimentation predictions are to be made for channels and trenches which are oblique (at an angle) to the approaching current (see Figure 10).

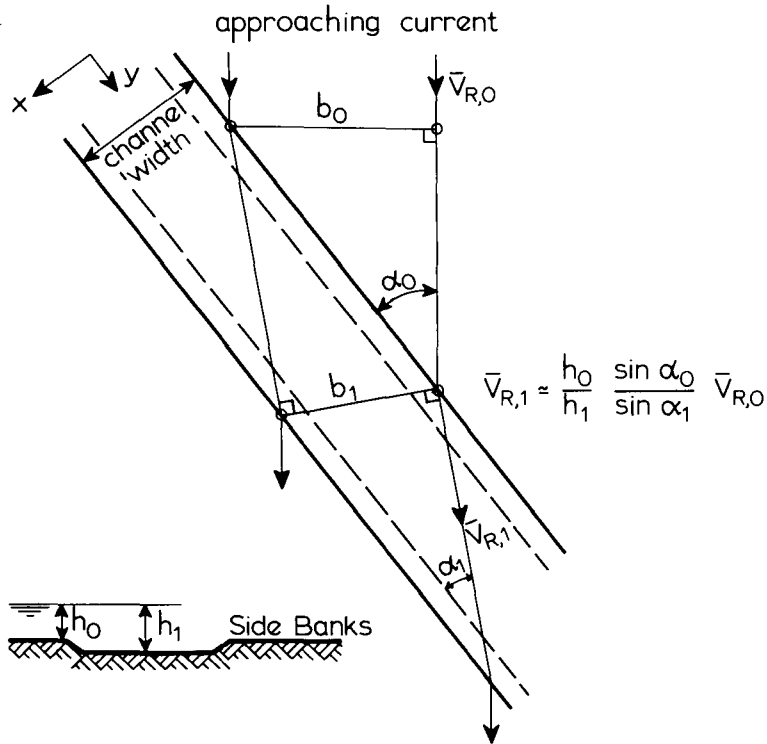


Figure 10 Streamline refraction in an oblique channel.

The streamlines are refracted at the upstream and downstream side slopes of the channel. The refraction effect is largest near the bed and smallest near the water surface. Because of the refraction effect, there is an increase of the current velocity within the channel (converging streamlines). For a channel at a small angle ( $\alpha_0 < 20^\circ$ ) the current velocity in the channel may become larger than that outside the channel.

The depth-averaged current velocity in an oblique channel of infinite length in ( $y$ -direction) can be described by the following equations:

$$\text{CONTINUITY} \quad \frac{\partial(h\bar{u})}{\partial x} = 0 \quad (8.1)$$

$$\text{MOTION} \quad u \frac{\partial \bar{u}}{\partial x} + \frac{1}{\rho} \frac{\partial \bar{p}}{\partial x} - g s_x + \frac{\bar{\tau}_{b,x}}{\rho h} = 0 \quad (8.2)$$

$$\bar{u} \frac{\partial \bar{v}}{\partial x} - g s_y + \frac{\bar{\tau}_{b,y}}{\rho h} = 0 \quad (8.3)$$

in which:

$\bar{u}$ = depth-averaged velocity in $x$ -direction	(m/s)
$\bar{v}$ = depth-averaged velocity in $y$ -direction	(m/s)
$\bar{p}$ = depth-averaged fluid pressure	(N/m <sup>2</sup> )
$\bar{\tau}_b$ = bottom shear stress (= $\rho g \bar{v}_R^2 / C^2$ )	(N/m <sup>2</sup> )
$s$ = bottom gradient	(-)
$h$ = water depth	(m)
$\rho$ = fluid density	(kg/m <sup>3</sup> )
$g$ = acceleration of gravity	(m/s <sup>2</sup> )

Boer (1984) has shown that both the convection and friction terms are of essential importance for a good representation of the flow field.

A numerical solution of Equations (8.1), (8.2) and (8.3) is also given by Boer (1984). Applying this approach the  $\bar{u}$  and  $\bar{v}$ -variables as well as the local current direction can be computed.

The current velocities along the refracted streamline can be represented in the SUTRENCH-model by varying the width ( $b$ ) of the flow.

## 9 Sensitivity analysis of controlling parameters of SUTRENCH-model

### 9.1 Introduction

A detailed sensitivity analysis of the controlling parameters of the SUTRENCH-model is given by van Rijn (1984). In this report only the influence of the most essential parameters, is given which are:

- the flow, wave and sediment transport conditions at the inlet ( $x = 0$ )
- the direction of the approaching current and the streamline refraction effects in the dredged channel,
- the particle fall velocity of the suspended sediment.

These controlling parameters should be based as much as possible on reliable and accurate measurements (field survey).

### 9.2 Influence of hydraulic conditions at the inlet

Generally, the inaccuracy of the sediment concentration profiles to be used as boundary conditions at the inlet ( $x = 0$ ) is rather large because of inadequate

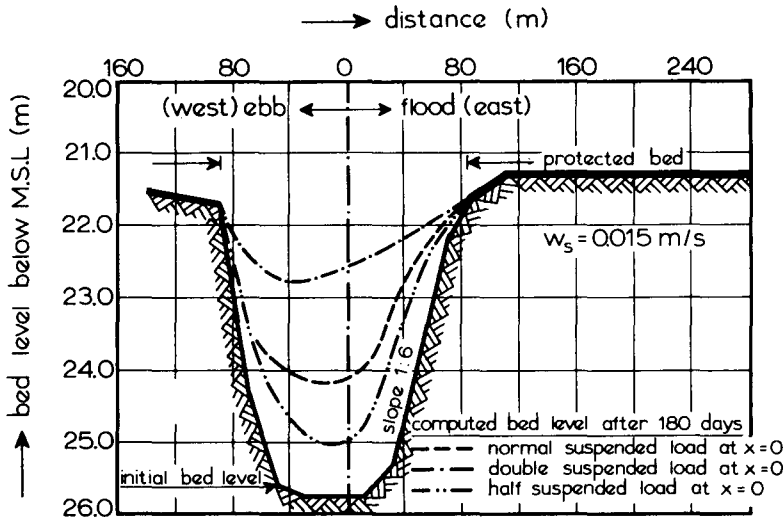


Figure 11 Influence of suspended load at the inlet on computed bed level (tidal flow).

measuring methods, tidal (neap-spring) and/or seasonal (summer-winter) fluctuations. Variations of a factor 2 are commonly observed values. When detailed measurements are not available, the flow and sediment transport conditions at the inlet ( $x = 0$ ) have to be estimated. In that case the inaccuracy may be much larger than a factor 2.

Figure 11 shows the influence of the suspended sediment transport at the inlet for a channel perpendicular to the (tidal) flow conditions in the Eastern Scheldt Estuary (The Netherlands). The variation of the suspended load is assumed to be a factor 2. As can be observed, the influence of variations of the suspended load on the computed bed level profiles is rather large. The amount of deposited material is almost linearly dependent on the value of the incoming suspended load.

Figure 12 shows the influence of the ratio of the suspended ( $s_s$ ) and total load ( $s_t = s_s + s_b$ ) at the inlet ( $x = 0$ ). The total load is  $s_t = 0.04 \text{ kg/sm}$  for all three computations. A large value of the suspended load ( $s_s/s_t = 0.9$ ) yields the largest sedimentation in the middle of the channel, but a less rapid migration of the upstream side slope. These results emphasize the importance of a correct estimation of the suspended and bed load at the inlet boundary.

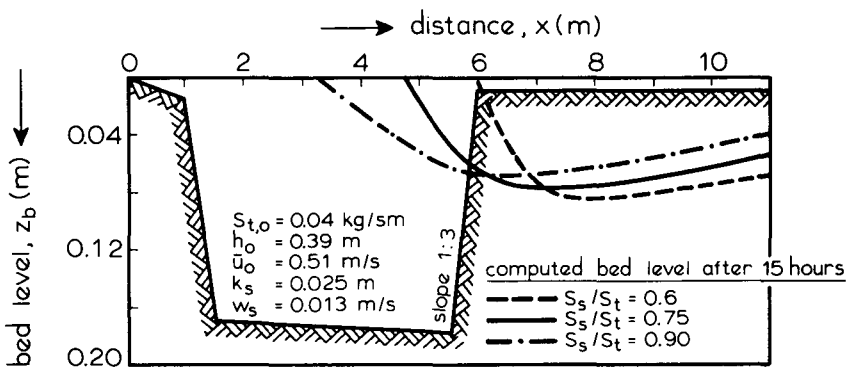


Figure 12 Influence of ratio of suspended and total load on computed bed level (unidirectional flow).

Finally, the influence of the wave height on the sediment transport at the inlet is presented. Generally, wave propagation models starting at deep water (boundary conditions) are used to predict the local wave height, when local measurements are not available. Depending on the complexity of the bed topography, the inaccuracy of the predicted local wave height may be as large as 20%. Figure 13 shows the computed bed levels for a 20% variation of the wave height at the inlet. The wave height in the channel is assumed to be equal to that at the inlet ( $x = 0$ ). A change of the incoming wave height results in a change of the incoming sediment transport and hence a change of the sedimentation rate in the channel.

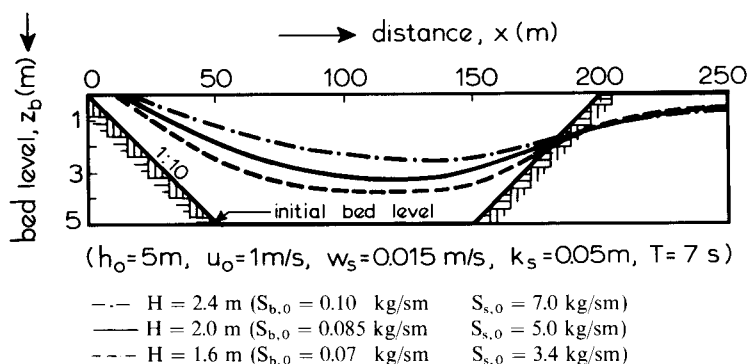


Figure 13 Influence of wave height on computed bed level (unidirectional flow).

### 9.3 Influence of streamline refraction

To investigate the influence of the refraction effects on the sedimentation in a channel oblique to the approaching flow, SUTRENCH-computations were carried out along *refracted* und *unrefracted* streamlines. The boundary conditions at the inlet were the same for all computations. The wave height was assumed to be constant. The streamline refraction was computed numerically (see chapter 8).

Figure 14 shows the current direction ( $\alpha$ ), the current velocity ( $\bar{v}_R$ ), the suspended load transport ( $S_s$ ) integrated over the width of the streamtube, and the bed levels for an approach angle of  $\alpha_0 = 10^\circ$ . The bed levels have been computed for an unidirectional flow and for a symmetrical tidal flow. The tidal flow is represented by two quasi-steady periods of 4 hours each.

Firstly, the computation along the *refracted* streamline is discussed.

The mean current velocity along the refracted streamline shows an increase from 1 m/s to 1.35 m/s at the downstream side slope. Because of the increasing velocities the reduction of the suspended load (resulting in sedimentation), which is mainly caused by contraction of the streamtube, is relatively small and confined to a region upstream of the channel axis. Downstream of the channel axis the suspended load transport increases resulting in erosion. This is clearly demonstrated by the computed bed level for unidirectional flow showing sedimentation upstream of the channel axis and erosion downstream of the channel axis. Similar patterns were observed in model tests carried out at the H.R.S. Wallingford (1973). Experiments with polystyrene particles (in suspension) in a channel with a rigid bottom showed sedimentation upstream of the channel axis while the region downstream of the channel axis remained free of polystyrene particles.

In case of symmetrical tidal flow the computed bed level shows erosion in the middle of the channel; the sediment material deposited during flood is removed

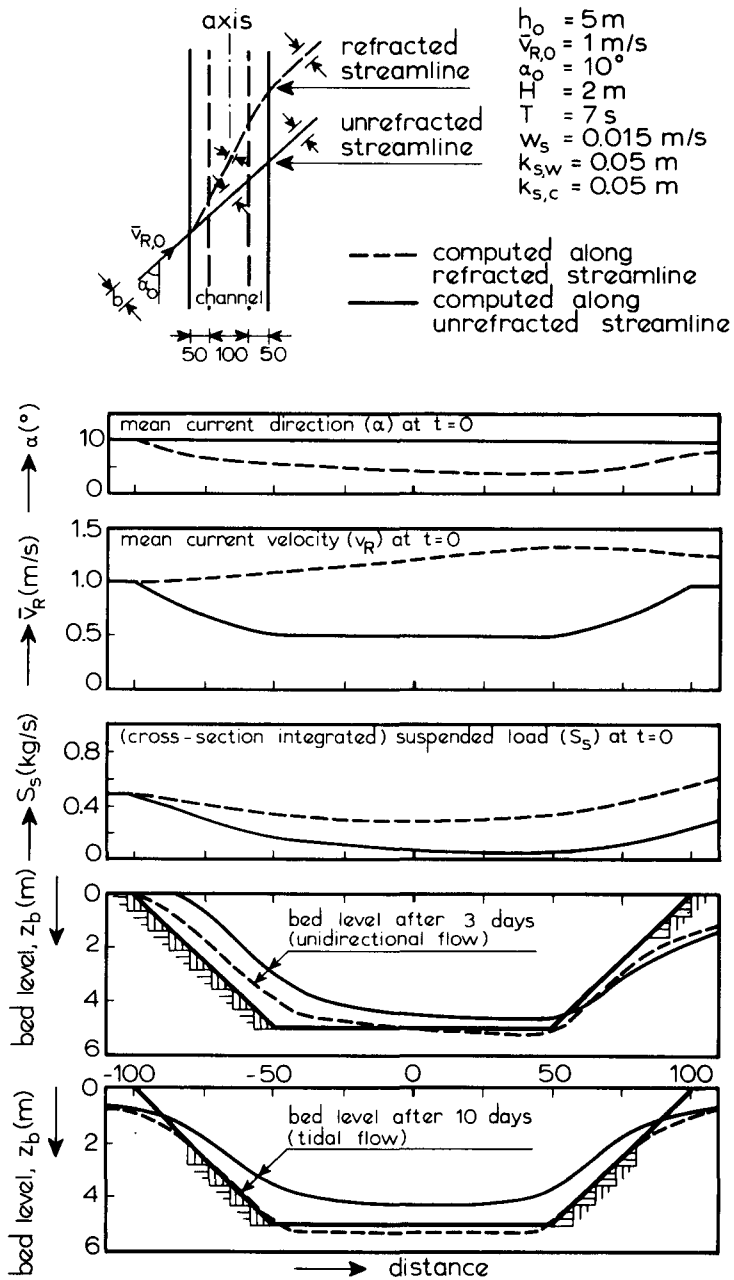


Figure 14 Influence of streamline refraction on sedimentation in a channel oblique to the flow ( $\alpha_0 = 10^\circ$ ).

during the ebb flow. Erosion can also be observed on both ends of the side slopes. Based on the above-given computation (along the *refracted* streamline), it seems that a channel inclined at an angle of  $10^\circ$  would not only be self-cleansing but self-deepening as well. This is not credible because man-made channels always show sedimentation of material. This must be attributed to secondary effects such as infill of bed-load particles due to the gravity component causing the particles to be deflected towards the channel axis, lateral diffusion and asymmetrical tidal flow. However, the overall sedimentation rate will be rather small because of the effect of increasing velocities in case of a small approach angle ( $\alpha_0 = 0$  to  $20^\circ$ ).

The computation along the *unrefracted* streamline shows a decrease of the mean current velocity because the current velocity is inversely proportional to the flow depth resulting in a considerable sedimentation (Fig. 14). Comparing the results for refracted and unrefracted streamlines, it is evident that the refraction effect cannot be neglected for an approach angle of  $\alpha_0 = 10^\circ$ .

Similar computations have been carried out for an approach angle of  $45^\circ$  and  $60^\circ$  (van Rijn, 1984). Based on these results, it seems acceptable to neglect the refraction effect for an approach angle between  $\alpha_0 = 60^\circ$  and  $\alpha_0 = 90^\circ$ .

#### 9.4 Influence of particle fall velocity of suspended sediment

Usually, the representative particle fall velocity is determined from suspended sediment samples using a (laboratory or in-situ) settling tube method. For sand

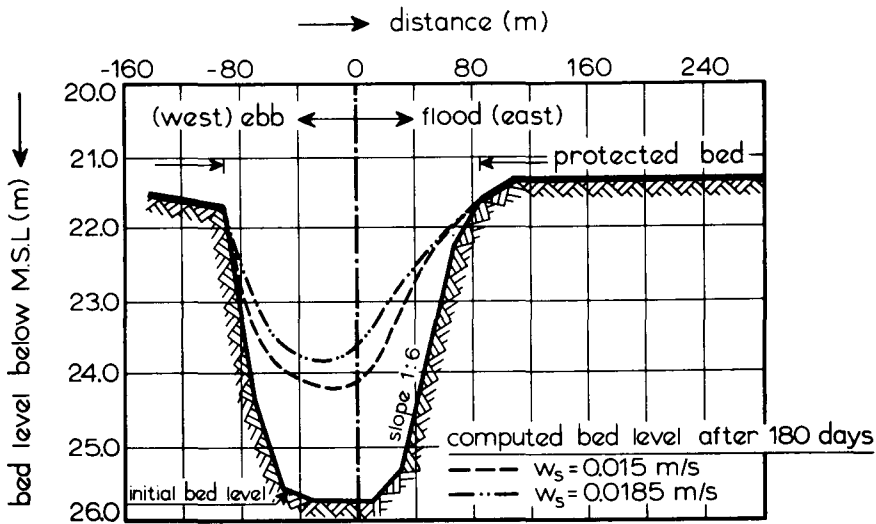


Figure 15 Influence of particle fall velocity on computed bed level (tidal flow).

particles the overall inaccuracy may be as large as 25%. For silt particles the inaccuracy may be much larger (say 50%). Figure 15 shows the influence of a 25% -increase of the particle fall velocity on the computed bed level for a channel perpendicular to the (tidal) flow conditions. The increase of the total amount of deposited material is about 25%.

Figure 16 shows the influence of a 20%-increase of the particle fall velocity on the computed bed level for a channel in an unidirectional flow. A larger particle fall velocity yields a smaller value of the suspended load in the channel and hence a larger sedimentation rate resulting in a more rapid migration of the upstream side slope.

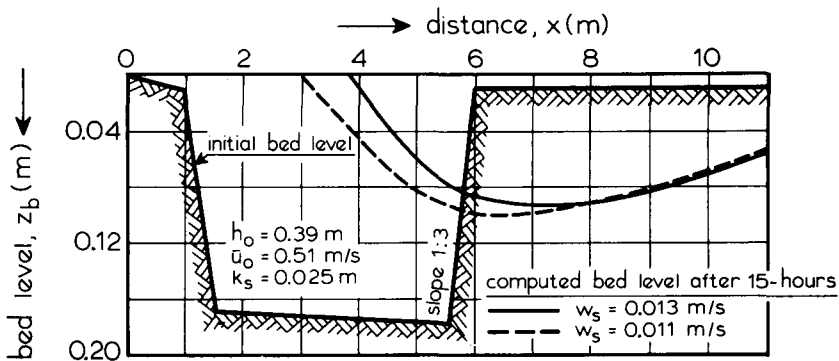


Figure 16 Influence of particle fall velocity on computed bed level (unidirectional flow).

### 9.5 Influence of other parameters

Variations (within reasonable physical ranges) of other hydraulic parameters such as the bed roughness, mixing coefficients, standard deviation of the effective bed-shear stress and the angle of internal friction of the bed material particles do not seriously effect the long-term morphological changes. This is also valid for the type of bed-boundary condition (bed-concentration or sediment flux) and the reference level at which the bed-boundary condition is applied (van Rijn, 1984).

The influence of wave height variations (due to depth variations; shoaling effect) on the sedimentation rate has also been investigated. The effect on the long-term morphological changes is relatively small and may, therefore, be neglected.

## 10 Verification of SUTRENCH-model

### 10.1 Introduction

A comprehensive verification analysis of the SUTRENCH-model has been carried out for various hydraulic conditions (van Rijn, 1984).

Herein, the most important results for sedimentation in dredged channels are given. The following cases are considered:

- migration of a channel in a flume,
- sedimentation in a trial dredge channel in the Western Scheldt, The Netherlands,
- sedimentation in a tunnel trench in a tidal river near Rotterdam, The Netherlands,
- sedimentation in a trial dredge channel in Asan Bay, Korea.

### 10.2 Migration of a channel in a flume

#### HYDRAULIC CONDITIONS

The migration of a channel with steep side slopes of 1 : 3 was studied in a flume (length = 30 m, width = 0.5 m, depth = 0.7 m). The sand bed with a thickness of 0.2 m consisted of medium fine sand with a  $d_{50} = 160 \mu\text{m}$  and a  $d_{90} = 200 \mu\text{m}$ . In the measuring section a small channel was excavated (see Figure 17).

To maintain equilibrium conditions upstream of the channel (no scour or

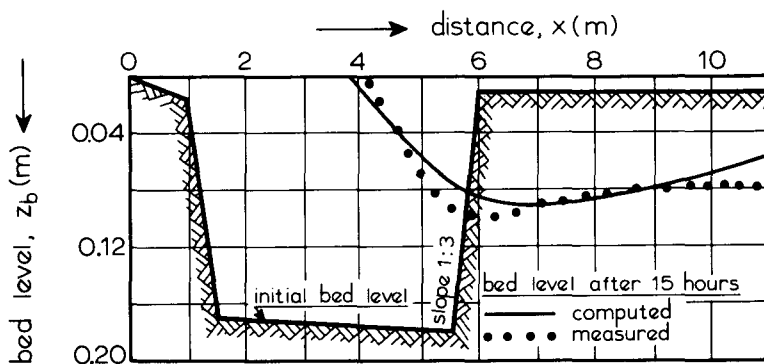


Figure 17 Migration of a channel in a flume.

deposition), sand of the same size and composition as the bed material was supplied at a constant rate of 0.04 kg/sm (Delft Hydraulics Laboratory, 1980b). The water depth at the inlet was 0.39 m. The current velocity at the inlet was 0.51 m/s. Measurements of the current velocities and sediment concentrations upstream of the channel were used to compute the suspended load resulting in a value of about 0.03 kg/sm. Hence, the bed-load transport was about 0.01 kg/sm (sand feed = total load = 0.04 kg/sm).

Based on the analysis of suspended sediment samples, the representative size of the suspended sediment was estimated to be 130  $\mu\text{m}$  resulting in a particle fall velocity of  $w_s = 0.013$  m/s (temperature of 15°C). Small-scale bed forms with a height in the range 0.015 to 0.035 m and a length in the range 0.10 to 0.25 m were present upstream of the channel. The effective roughness of the movable bed was estimated to be  $k_s = 0.025$  m (from velocity profiles).

#### COMPUTATIONS

The SUTRENCH-model for complicated flows was used to compute the migration of the channel.

At the inlet boundary ( $x = 0$ ) the equilibrium concentration profile (based on measurements) was specified. The velocity profile at  $x = 0$  was described by a logarithmic profile. For these conditions the maximum value of the mixing coefficient at  $x = 0$  is  $\varepsilon_{max, 0} = 0.00155$  m<sup>2</sup>/s (Equation (4.5)).

The bed-boundary condition was specified at a level of  $a = 0.0125$  m applying the  $E_a$ -method (Equation (5.9)). The coefficient of Equation (5.9) was adjusted somewhat to give a suspended load of  $s_s = 0.03$  kg/sm at  $x = 0$  (as measured). The coefficient of the bed-load formula (Equation (6.5)) was also adjusted to give  $s_b = 0.01$  kg/sm at  $x = 0$ . The porosity factor of the bed material was assumed to be 0.4. The numerical parameters were:  $\Delta x = 0.25$  m, 10 grid points in vertical direction,  $\Delta t = 900$  s, and  $\gamma_s = 0.8$ .

#### RESULTS

Figure 17 shows the migration of the channel after 15 hours. The agreement between measured and computed values is rather good.

### 10.3 Sedimentation in a trial dredge channel in the Western Scheldt, The Netherlands

#### HYDRAULIC CONDITIONS

In 1965 a pipe line channel was dredged across the Westerschelde (Western Scheldt), a tidal estuary in the southwest part of the Netherlands. The channel axis

was almost perpendicular to the flow. To estimate the sedimentation rate, a trial channel was dredged perpendicular to the tidal flow. A typical cross-section with measured bed-level profiles is shown in Figure 18.

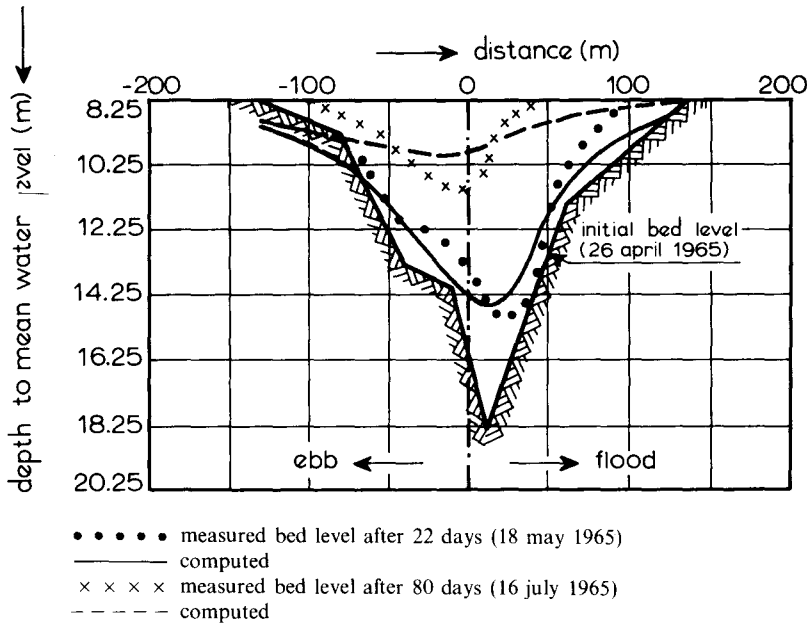


Figure 18 Trial dredge channel in Western Scheldt, The Netherlands.

The local hydraulic conditions during the mean tide are shown in Figure 19.

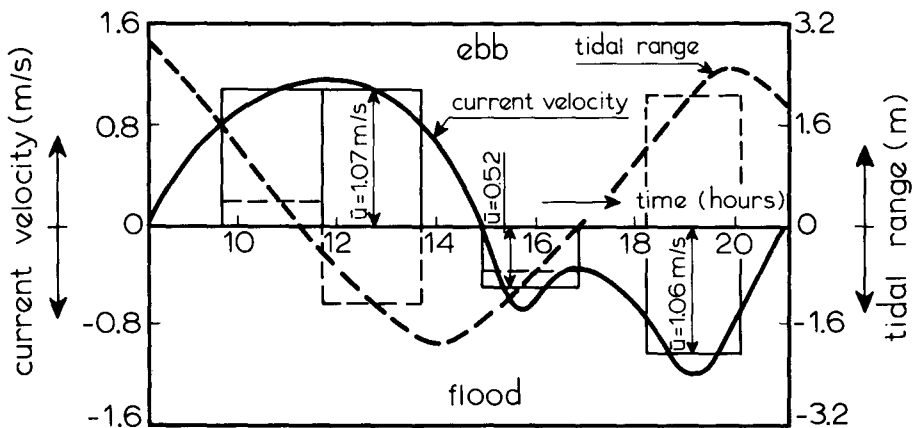


Figure 19 Hydraulic (tidal) conditions.

The bed material consisted of sand ( $d_{50} = 180 \mu\text{m}$ ,  $d_{90} = 220 \mu\text{m}$ ). The representative particle diameter of the suspended sediment was estimated to be about  $140 \mu\text{m}$  resulting in a particle fall velocity of  $w_s = 0.015 \text{ m/s}$  (temperature  $15^\circ\text{C}$ ). The effective bed roughness was estimated to be  $k_s = 0.2 \text{ m}$  (local bed-form height  $\approx 0.2 \text{ m}$ ).

Flow velocity and sand concentration measurements were carried out to determine the suspended load transport.

The inaccuracy of the suspended load may be rather large (say  $\pm 50\%$ ) because of seasonal variations, inaccuracy of measuring methods and systematic errors (lag effects). The bed-load transport was not measured.

#### COMPUTATIONS

The SUTRENCH-model for complicated flows was used to compute the bed level profiles at various times. The neap-spring tidal cycle was represented by the mean tide. The mean tidal cycle was schematized to 4 quasi-steady flow periods of 2 hours each (Figure 19). The periods with small velocities (below initiation of motion) near slack tide were neglected.

To represent the sediment transport during the neap-spring cycle correctly, the current velocities of the mean tidal cycle should be increased slightly (5 to 10%). In this way the relatively large contribution to the sediment transport by the springtide velocities can be accounted for, as shown by Van Rijn (1984). Assuming a power-law relationship with an exponent of 3 ( $s \approx \bar{u}^3$ ) between the sediment transport ( $s$ ) and the mean current velocity ( $\bar{u}$ ), the velocities of the mean tide should be multiplied by a factor 1.05. Usually, this effect is negligibly small compared with the inaccuracy of the incoming sediment transport. Equilibrium concentration profiles are specified at the inlet ( $x = 0$ ). The velocity profiles at  $x = 0$  are assumed to have a logarithmic distribution. As bed-boundary condition the  $E_a$ -method (Equation 5.9)) has been used at a level of  $a = 0.1 \text{ m}$  above the bed. The coefficient of Equation (5.9) has been adjusted to give the correct measured suspended sand transport at  $x = 0$ . The bed-load transport is computed by Equation (6.5). The porosity factor of the bed material is assumed to be 0.4.

The numerical parameters are, as follows:  $\Delta x = 5 \text{ m}$ , 10 grid points in vertical direction,  $\Delta t = 7200 \text{ s}$ ,  $\gamma_s = 0.2$ .

#### RESULTS

Figure 18 shows measured and computed bed levels. The computed sedimentation rates are reasonably good. It may be noted that the measured profiles donot show erosion at the banks.

## 10.4 Sedimentation in a tunnel trench in a tidal river near Rotterdam, The Netherlands

### HYDRAULIC CONDITIONS

In 1978 a tunnel trench was dredged perpendicular to the flow in a small tidal river near Rotterdam (Botlek-tunnel in Oude Maas). A typical cross-section in the middle of the river is shown in Figure 20.

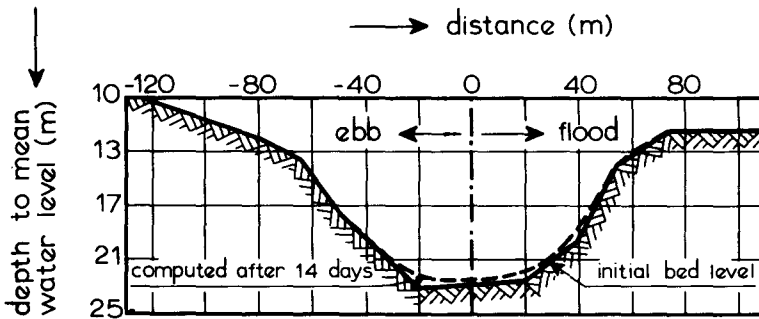


Figure 20 Tunnel trench in a tidal river near Rotterdam.

The hydraulic conditions are dominated by the river flow resulting in a dominating ebb period of about 6 hours (current velocity of about 0.9 m/s, water depth of about 11 m). The effective flood period is about 4 hours (current velocity of about 0.6 m/s, water depth of about 10 m). The bed consisted of fine sandy material ( $d_{50} = 200 \mu\text{m}$ ,  $d_{90} = 300 \mu\text{m}$ ). Based on suspended sediment samples, the representative particle diameter of the suspended sand was estimated to be about  $110 \mu\text{m}$  resulting in a particle fall velocity of 0.01 m/s (temperature of  $15^\circ\text{C}$ ). The effective bed roughness was estimated to be about 0.15 m. Flow velocity and sediment concentration measurements were carried out to determine the suspended sediment transport. The bed load was not measured.

### COMPUTATIONS

The SUTRENCH-model for complicated flows was used to compute the sedimentation in the trench. The applied boundary conditions are similar to those reported in paragraph 10.3. The wash or silt load was not taken into account because its contribution to the sedimentation process was assumed to be of minor importance. The numerical parameters are, as follows:  $\Delta x = 5 \text{ m}$ , 10 grid points in vertical direction,  $\Delta t = 7200 \text{ s}$ ,  $\gamma_s = 0.05$ .

## RESULTS

Figure 20 shows the computed bed level after 14 days. The sedimentation in the deepest part of the trench (over a length of about 25 m on both sides of the axis) is about  $25 \text{ m}^3$  per unit width. This value can be compared with the maintenance dredging volume of about 10 to  $20 \text{ m}^3$  per unit width during a period of 14 days in the same part of the trench.

### 10.5 Sedimentation in a trial dredge channel in Asan Bay, Korea

#### HYDRAULIC CONDITIONS

To obtain information of the annual sedimentation rate in a (planned) shipping channel in the Asan Bay of Korea, a trial dredge channel (length of about 750 m, width of about 150 m, Figure 21 A) was dredged in the summer period of 1983. The initial bed profile along the (refracted) streamline in the channel is shown in Figure 21 D.

To determine the streamline pattern in the channel, a physical scale model (fixed bed) as well as a mathematical model was operated. Based on the model results, the approach angles of the currents were found to be  $\alpha_0 = 20^\circ$  for the flood phase and  $\alpha_0 = 15^\circ$  for the ebb phase. The current direction in the channel was found to be  $\alpha = 10^\circ$  for the flood as well as the ebb phase. Analysis of tide data showed a semi-diurnal type with a small diurnal inequality. The mean tidal range is about 6 m. Maximum current velocities were in the range 0.6 to 1.2 m/s during the neap-spring tidal cycle.

Analysis of wave data for the summer period showed a significant wave height of about 0.5 m for the flood phase and of about 0.25 for the ebb phase. The wave period was about 4 s.

Analysis of various bed material samples showed the presence of medium fine sand with a median ( $d_{50}$ ) particle diameter of  $200 \mu\text{m}$ . Data of suspended sand concentrations were not available. Analysis of echo soundings showed the presence of bed forms with a length of about 25 to 50 m, and a height of about 0.25 to 0.50 m. Detailed information is reported by the Ministry of Construction of the Republic of Korea (1983).

#### COMPUTATIONS

The SUTRENCH-model for current and waves was used to compute the bed level changes of the trial dredge channel over a period of 100 days. The mean tidal cycle

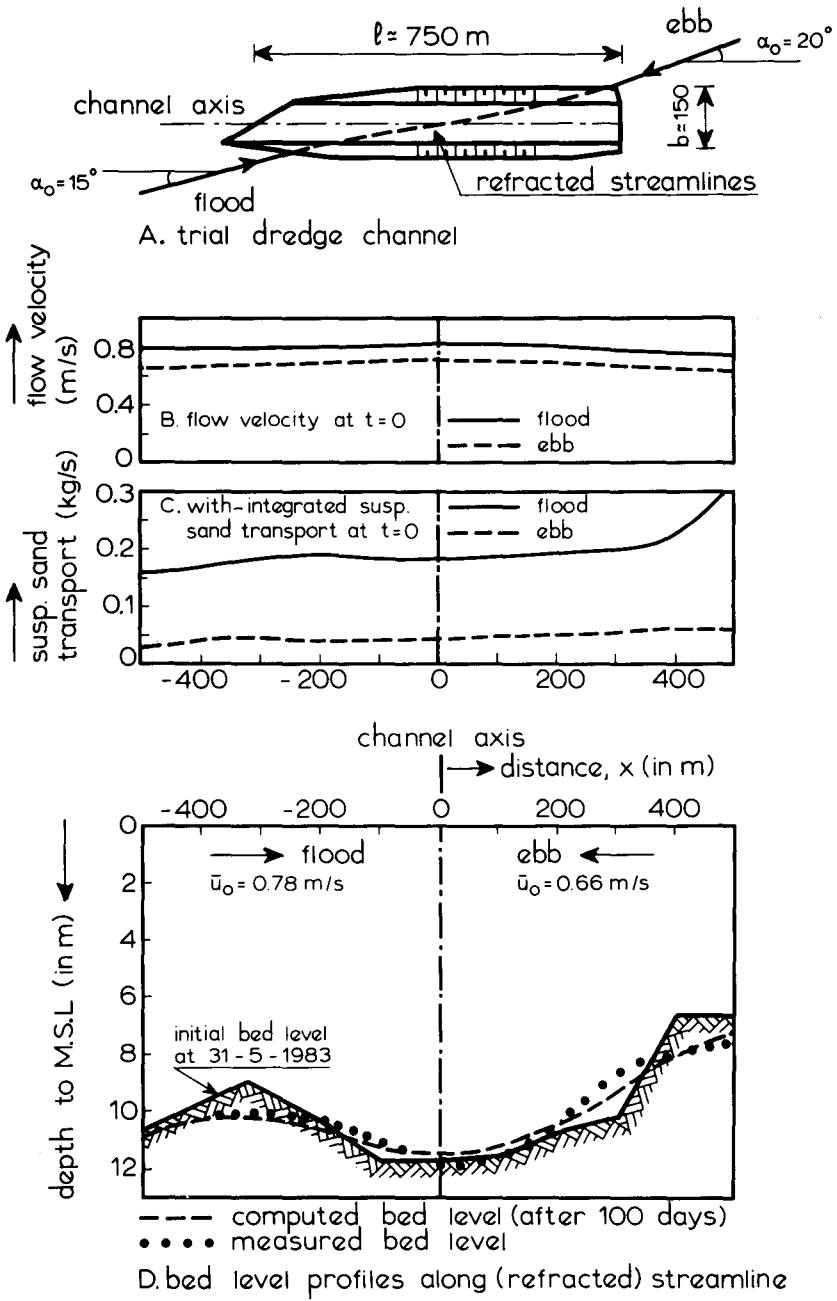


Figure 21 Trial dredge channel in Asan Bay, Korea.

was schematized to 2 quasi-steady flow periods of 6 hours each. The characteristic approach current velocities were 0.78 m/s for the flood phase and 0.66 m/s for the ebb phase. The water depth at the inlet during flood was about 11 m and about 6.7 m during ebb.

Because the channel is oblique to the approaching flow field, streamline refraction in the channel will occur. The direction of the refracted streamlines and the magnitude of the current velocities along the refracted streamlines were computed by applying a two-dimensional horizontal mathematical model for an oblique channel of infinite length (see chapter 8).

The predicted velocities were reduced slightly (10%) to account for the finite length of the trial dredge channel. The SUTRENCH-model was applied along a refracted streamline. The current velocities were represented by varying the width of the flow (streamtube approach). The computed current velocities, presented in Figure 21B, show a small increase of the velocities in the channel.

At the inlet boundary ( $x = 0$ ) equilibrium concentration profiles were specified. Standard coefficients were used. Data for calibration were not available. The representative particle diameter of the suspended sand material was estimated to be about 150  $\mu\text{m}$  resulting in a fall velocity of about  $w_s = 0.016$  m/s ( $Te \simeq 20^\circ\text{C}$ ).

As bed-boundary condition the  $E_a$ -method was used, applied at a level of 0.15 m above the mean bed. The effective roughness was assumed to be  $k_s = 0.15$  m.

The bed-load transport was computed by Equation (6.4).

Sedimentation of bed-load particles by gravity infill from the side slopes was neglected.

The numerical parameters are:  $\Delta x = 25$  m, 10 grid points in vertical direction,  $\Delta t = 21600$  s,  $\gamma_s = 0.1$ .

## RESULTS

Figure 21C shows the width-integrated suspended sand transport (at  $t = 0$ ) for the flood and ebb phase of the tide. The flood phase is the dominant period for the sediment transport. Figure 21D shows measured and computed bed levels after a period of 100 days. The agreement is rather good, particularly at the banks of the channel where erosion can be observed. In the middle of the channel there is also a small region with erosion, probably caused by relatively large current velocities. This effect was not predicted by the SUTRENCH-model. The reason for this may be an underprediction of the current velocities in the channel.

# 11 Sediment trapping efficiency of dredged channels and trenches

## 11.1 Introduction

To obtain simple rules for sedimentation predictions, the SUTRENCH-model has been applied to determine the trapping efficiency of dredged channels with various dimensions and approach angles, as shown schematically in Figure 22. The channel is assumed to be infinitely long (along the axis). Streamline refraction in the channel has been computed numerically, as presented in chapter 8, resulting in the magnitude and direction of the current velocity vector at each location. These

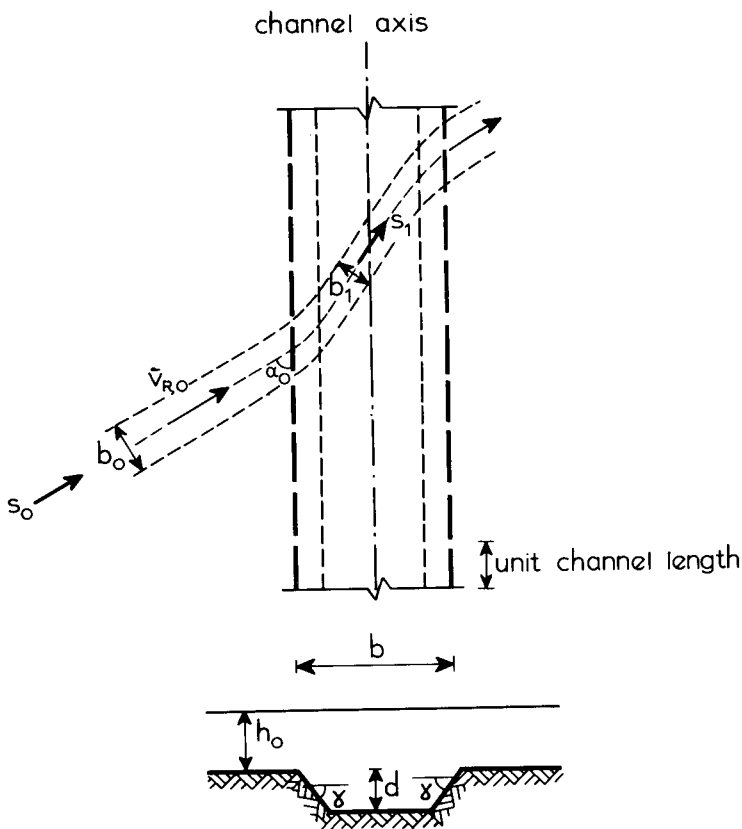


Figure 22 Definition sketch for sediment trapping efficiency of dredged channels.

results have been specified to the SUTRENCH-model (streamtube approach). Based on this, the SUTRENCH-model computes the suspended sediment transport along the streamtube.

## 11.2 Computations

In all, 300 computations have been executed using the following data (see also Figure 22):

approach current velocity	: $\bar{v}_{R,0}$ = 1 m/s
approach water depth	: $h_0$ = 5 m
approach angles	: $\alpha_0$ = 15°, 30°, 60° and 90°
channel depth	: $d$ = 2, 2.5, 5 and 10 m
channel width (normal to axis)	: $b$ = 50, 100, 200 and 500 m
channel side slope (normal to axis)	: $\tan \gamma$ = 1 : 5, 1 : 10 and 1 : 20
particle fall velocity	: $w_s$ = 0.0021, 0.005, 0.0107, 0.0142, 0.025 and 0.036
effective bed roughness	: $k_s$ = 0.2 m

## 11.3 Results

The trapping efficiency ( $e$ ) is defined as the relative difference of the incoming suspended sediment transport and the minimum value of the suspended sediment transport in the channel:

$$e = \frac{b_0 s_0 - (b_1 s_1)_{\text{minimum}}}{b_0 s_0} \quad (1.11)$$

in which:

$b_0$ = approach width of streamtube	(m)
$b_1$ = width of streamtube in channel	(m)
$s_0$ = incoming suspended sediment transport per unit width	(kg/sm)
$s_1$ = suspended sediment transport per unit width in channel	(kg/sm)

The basic parameters which determine the trapping efficiency are: the approach angle ( $\alpha_0$ ), approach velocity ( $\bar{v}_{R,0}$ ) and depth ( $h_0$ ), approach bed-shear velocity ( $u_{*,0}$ ), particle fall velocity ( $w_s$ ), channel depth ( $d$ ), channel width ( $b$ ) and channel side slope ( $\tan \gamma$ ).

The functional relationship is:

$$e = F(\alpha_0, \bar{v}_{R,0}, \frac{w_s}{u_{*,0}}, \frac{d}{h_0}, \frac{b}{h_0}, \tan \gamma) \quad (11.2)$$

Figure 23 presents the results for a channel perpendicular ( $\alpha_0 = 90^\circ$ ) to the flow direction. These results show that the influence of the side slope angle ( $\gamma$ ) is negligibly small.

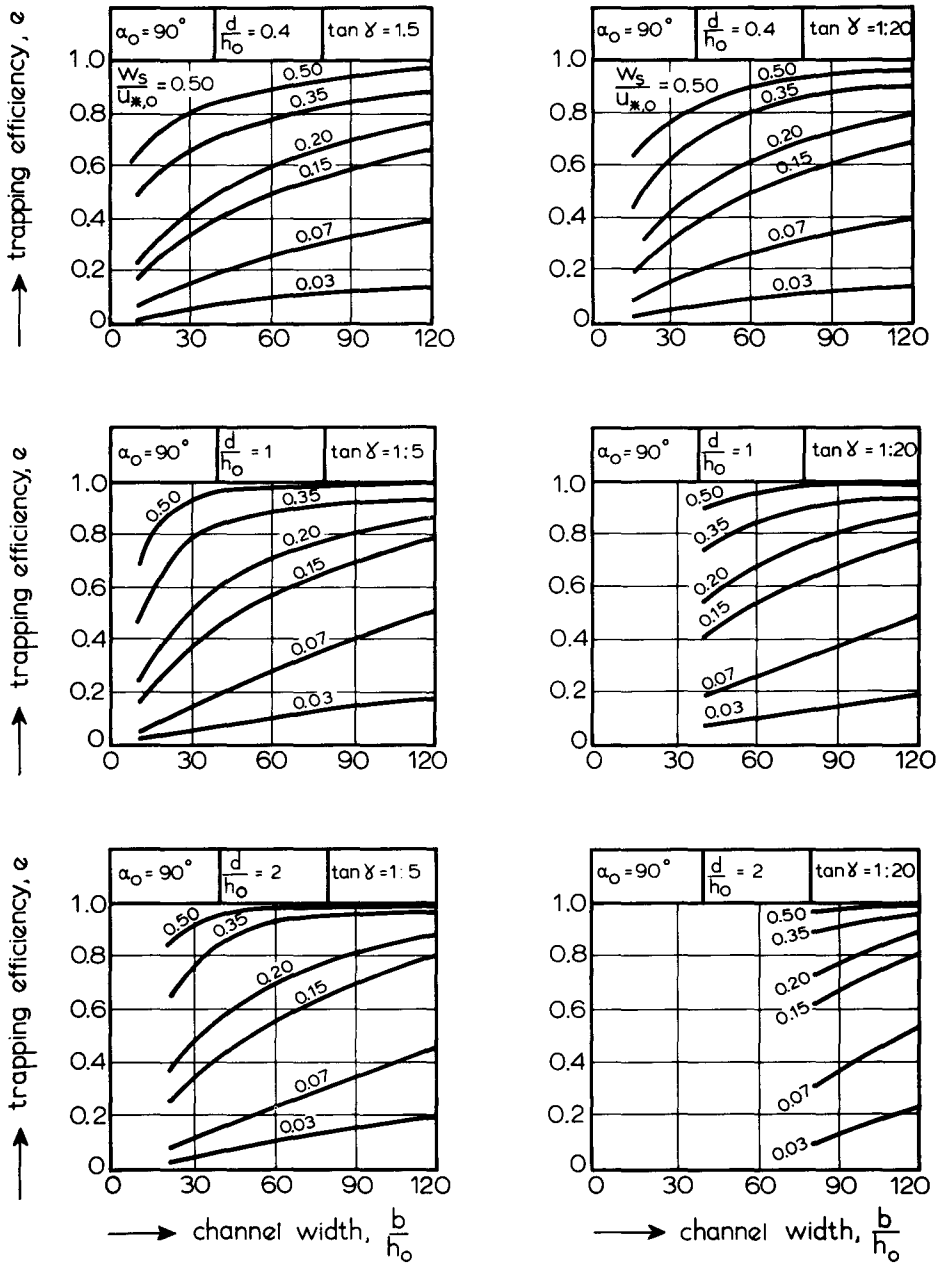


Figure 23 Sediment trapping efficiency of a channel perpendicular to the flow ( $\alpha_0 = 90^\circ$ ).

Additional results for oblique channels are given by van Rijn (1984). The sedimentation rate (in kg/sm) per unit channel length (along the axis) immediately after dredging can be computed by (see Figure 22):

$$D = e s_0 \sin \alpha_0 \quad (11.3)$$

Finally, it is noted that this simple approach only yields a rough estimate of the sedimentation rate, which should not be used for detailed feasibility and economical studies of shipping channels.

## 12 References

- ALFRINK, B.J. and RIJN, L.C. van, 1983, Two-Equation Turbulence Model for Flow in Trenches, Journal of Hydraulics Division, ASCE, vol. 109, No. 3, USA.
- BOER, S., 1984, The Flow across Trenches at Oblique Angle to the Flow, Delft Hydraulics Laboratory, Report S490, Delft, The Netherlands.
- COLEMAN, N.L., 1970, Flume Studies of the Sediment Transfer Coefficient, Water Resources Research, Vol. 6, No. 3, USA.
- COLES, D., 1965, The Law of the Wake in the Turbulent Boundary Layer, Journal of Fluid Mechanics, Vol. 1, England.
- DELFT HYDRAULICS LABORATORY, 1975, Sedimentation of Tunnel Trenches (in Dutch), Report R975-I, Delft, The Netherlands.
- DELFT HYDRAULICS LABORATORY, 1977, Numerical Model for Non-Steady Suspended Sediment Transport Report R975-II, Delft, The Netherlands.
- DELFT HYDRAULICS LABORATORY, 1980b, Computation of Siltation in Dredged Trenches, Report R1267-III, Delft, The Netherlands.
- DELFT HYDRAULICS LABORATORY, 1980b, Computation of Siltation in Dredged Trenches, Report R1267-V, Delft, The Netherlands.
- DELFT HYDRAULICS LABORATORY, 1981a, Entrainment of Fine Sediment Particles; Determination of Bed-shear Velocities, Report M1531-I, Delft, The Netherlands.
- DELFT HYDRAULICS LABORATORY, 1981b, Entrainment of Fine Sediment Particles; Development of Concentration Profiles in a Steady Uniform Flow without Initial Sediment Load, Report M1531-II, Delft, The Netherlands.
- DELFT HYDRAULICS LABORATORY, 1983a, Entrainment of Fine Sediment Particles; Initiation of Motion and Suspension, Development of Concentration Profiles in a Steady Uniform Flow without Initial Sediment Load, Report M1531-III, Delft, The Netherlands.
- DELFT HYDRAULICS LABORATORY, 1983b, Entrainment of Fine Sediment Particles; Sediment Pick-up Functions, Report M1531-IV, Delft, The Netherlands.
- HJELMFELT, A.T. and LENAU, C.W., 1970, Non-Equilibrium Transport of Suspended Sediment, Journal of the Hydraulics Division, ASCE, HY 7, USA.
- H.R.S. WALLINGFORD, 1973, Laboratory Studies of Flow across Dredged Channels, Report EX 618, Wallingford, England.
- KERSSENS, P.J.M., 1977, Morphological Computations for Suspended Sediment Transport, Delft Hydraulics Laboratory, Report S78-VI, The Netherlands.
- KERSSENS, P.J.M., PRINS, A. and RIJN, L.C. van, 1979, Model for Suspended Sediment Transport Journal of the Hydraulics Division, ASCE, HY 5, USA.
- KERSSENS, P.J.M. and RIJN, L.C. van, 1977, Model for Non-Steady Suspended Sediment Transport 18th IAHR-congress, Baden-Baden, West-Germany.
- REPUBLIC OF KOREA, Ministry of Construction, 1983, Sedimentation Study for Navigation Channel of the Pyeong Teak LNG Receiving Terminal, Volume I.
- RODI, W., 1980, Turbulence Models and their Application in Hydraulics, IAHR-section on Fundamentals of Division II, Delft, The Netherlands.
- RIJN, L.C. van, 1980, Model for Sedimentation Predictions, 19th IAHR-congress, New Delhi, India.
- RIJN, L.C. van, 1981, Computation of Bed-load Concentration and Bed Load Transport, Delft Hydraulics Laboratory, Report, S487-I, Delft, The Netherlands.
- RIJN, L.C. van, 1982a, Computation of Bed Load and Suspended Load Transport, Delft Hydraulics Laboratory, Report, S487-II, Delft, The Netherlands.
- RIJN, L.C. van, 1982b, Prediction of Bed Forms, Alluvial Roughness and Sediment Transport, Delft Hydraulic Laboratory, Report, S487-III, Delft, The Netherlands.

- RIJN, L.C. van, 1983, Two-Dimensional Mathematical Flow Model with a Two-Equation Turbulence Closure, Delft Hydraulics Laboratory, Report S488-I, Delft, The Netherlands.
- RIJN, L.C. van, 1984, Two-dimensional Vertical Mathematical Modelling of Suspended Sediment by Current and Waves, Delft Hydraulics Laboratory, Report S488-IV, Delft, The Netherlands.
- RIJN, L.C. van, 1985, Initiation of Motion, Bed Forms, Bed Roughness, Sediment Concentration and Transport by Current and Waves, Delft Hydraulics Laboratory, Report S487-IV, Delft, The Netherlands.
- VREUGDENHIL, C.B., 1982, Numerical Solution of a Convection-Diffusion Equation using Finite Elements Delft Hydraulics Laboratory, Internal Note X 59, Delft, The Netherlands.

In the series of Rijkswaterstaat Communications the following numbers have been previously published:

- No. 1. *Tidal Computations in Shallow Water*  
Dr. J. J. Dronkers † and prof. dr. ir. J. C. Schönfeld  
*Report on Hydrostatic Leveling across the Westerschelde*  
Ir. A. Waalewijn, 1959
- No. 2. *Computations of the Decca Pattern for the Netherlands Delta Works*  
Ir. H. Ph. van der Schaaf † and P. Vetterli, Ing. Dipl. E. T. H., 1960
- No. 3. *The Aging of Asphaltic Bitumen*  
Ir. A. J. P. van der Burgh, J. P. Bouwman and G. M. H. Steffelaar, 1962
- No. 4. *Mud Distribution and Land Reclamation in the Eastern Wadden Shallows*  
Dr. L. F. Kamps †, 1962
- No. 5. *Modern Construction of Wing-Gates*  
Ir. J. C. le Nobel, 1964
- No. 6. *A Structure Plan for the Southern IJsselmeerpolders*  
Board of the Zuyder Zee Works, 1964
- No. 7. *The Use of Explosives for Clearing Ice*  
Ir. J. van der Kley, 1965
- No. 8. *The Design and Construction of the Van Brienoord Bridge across the River Nieuwe Maas*  
Ir. W. J. van der Eb †, 1968
- No. 9. *Electronic Computation of Water Levels in Rivers during High Discharges*  
Section River Studies. Directie Bovenrivieren of Rijkswaterstaat, 1969
- No. 10. *The Canalization of the Lower Rhine*  
Ir. A. C. de Gaay and ir. P. Blokland †, 1970
- No. 11. *The Haringvliet Sluices*  
Ir. H. A. Ferguson, ir. P. Blokland † and ir. drs. H. Kuiper, 1970
- No. 12. *The Application of Piecewise Polynomials to Problems of Curve and Surface Approximation*  
Dr. Kurt Kubik, 1971
- No. 13. *Systems for Automatic Computation and Plotting of Position Patterns*  
Ir. H. Ph. van der Schaaf †, 1972
- No. 14. *The Realization and Function of the Northern Basin of the Delta Project*  
Deltadienst of Rijkswaterstaat, 1973
- No. 15. *Fysical-Engineering Model of Reinforced Concrete Frames in Compression*  
Ir. J. Blaauwendraad, 1973
- No. 16. *Navigation Locks for Push Tows*  
Ir. C. Kooman, 1973
- No. 17. *Pneumatic Barriers to reduce Salt Intrusion through Locks*  
Dr. ir. G. Abraham, ir. P. van der Burg and ir. P. de Vos, 1973

- No. 18. *Experiences with Mathematical Models used for Water Quality and Water Problems*  
Ir. J. Voogt and dr. ir. C. B. Vreugdenhil, 1974
- No. 19. *Sand Stabilization and Dune Building*  
Dr. M. J. Adriani and dr. J. H. J. Terwindt, 1974
- No. 20. *The Road-Picture as a Touchstone for the three dimensional Design of Roads*  
Ir. J. F. Springer and ir. K. E. Huizinga (also in German), 1975
- No. 21. *Push Tows in Canals*  
Ir. J. Koster, 1975
- No. 22. *Lock Capacity and Traffic Resistance of Locks*  
Ir. C. Kooman and P. A. de Bruijn, 1975
- No. 23. *Computer Calculations of a Complex Steel Bridge verified by Model Investigations*  
Ir. Th. H. Kayser and ir. J. Brinkhorst, 1975
- No. 24. *The Kreekrak Locks on the Scheldt-Rhine Connection*  
Ir. P. A. Kolkman and ir. J. C. Slagter, 1976
- No. 25. *Motorway Tunnels built by the Immersed Tube Method*  
Ir. A. Glerum, ir. B. P. Rigter, ir. W. D. Eysink and W. F. Heins, 1976
- No. 26. *Salt Distribution in Estuaries*  
Rijkswaterstaat, Delft University of Technology, Delft Hydraulics Laboratory, 1976
- No. 27. *Asphalt Revetment of Dyke Slopes*  
Committee on the Compaction of Asphalt Revetments of Dyke Slopers, 1977
- No. 28. *Calculation Methods for Two-dimensional Groundwater Flow*  
Dr. ir. P. van der Veer, 1978
- No. 29. *Ten years of Quality Control in Road Construction in the Netherlands*  
Ir. C. van de Fliert and ir. H. Schram, 1979
- No. 30. *Digital Large Scale Restitution and Map Compilation*  
J. G. van der Kraan, H. Rietveld, M. Tienstra and W. J. H. IJzereef, 1980
- No. 31. *Policy Analysis for the National Water Management of the Netherlands*  
(Netherlands Contributions, related to the PAWN-study, for the ECE-seminar on Economic Instruments for the Rational Utilization of Water Resources - Veldhoven, Netherlands - 1980)
- No. 32. *Changing Estuaries*  
Dr. H. L. F. Saeijs, 1982
- No. 33. *A Bird's Eye View of the Shipping Traffic on the North Sea*  
North sea directorate, 1982
- No. 34. *Contributions to Remote Sensing: Applications of Thermal Infrared*  
H. W. Brunsveld van Hulten (ed.), P. Hoogenboom, A. F. G. Jacobs, C. Kraan, G. P. de Loor and L. Wartena, 1984
- No. 35. *On the Constuction of Computational Methods for Shallow Water Flow Problems*  
Dr. ir. G. S. Stelling, 1984

- No. 36. *Wrong-way driving*  
Ir. G. A. Brevoord
- No. 37. *The Use of Asphalt in Hydraulic Engineering*  
Technical Advisory Committee on Waterdefences, 1985
- No. 38. *Recycling of Road Pavement Materials in the Netherlands*  
J. J. Gerardu and C. F. Hendriks, 1985
- No. 39. *Groundwater Infiltration with Bored Wells*  
National Institute for Water Supply, et al, 1985
- No. 40. *Biological Research Ems-Dollard Estuary*  
Biological Study of the Ems-Dollard Estuary (BOEDE), 1985